

Fig. 1.

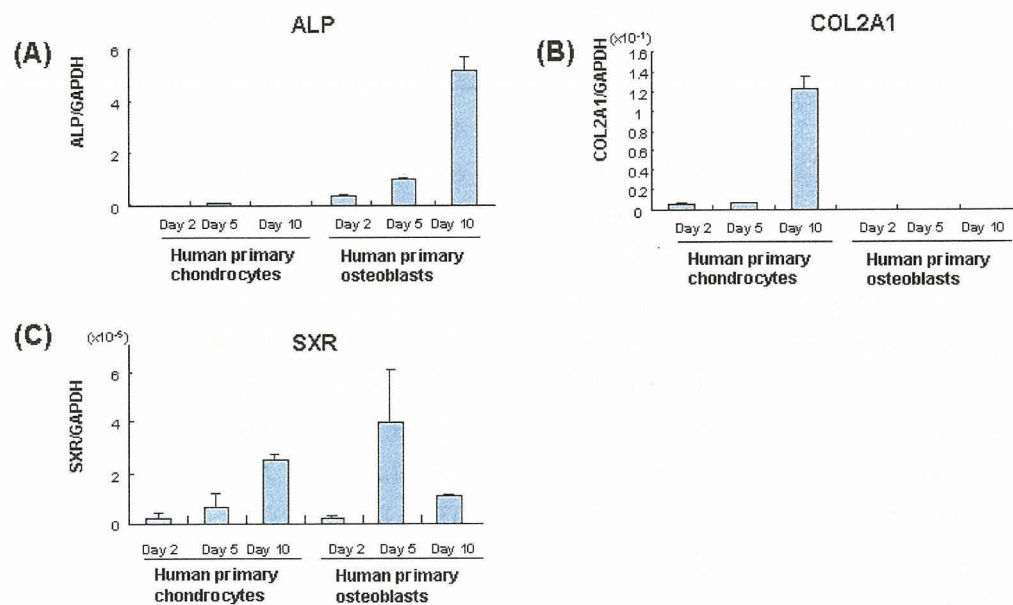
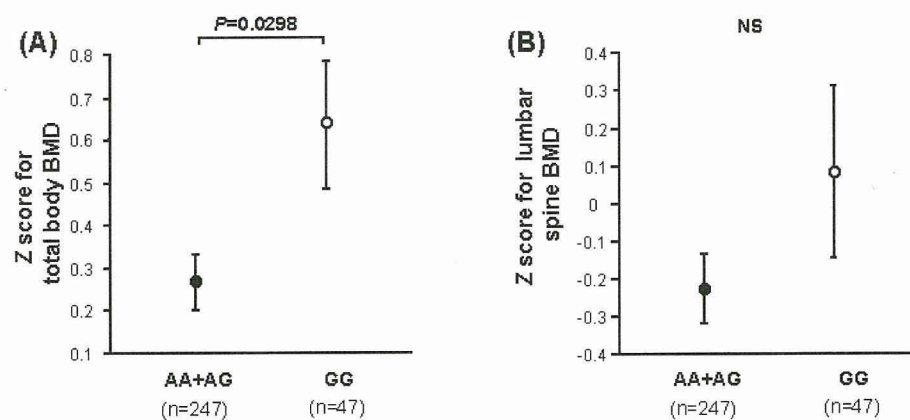


Fig. 2.



Carminerin contributes to chondrocyte calcification during endochondral ossification

Takashi Yamada¹, Hirotaka Kawano¹, Yu Koshizuka¹, Toru Fukuda², Kimihiro Yoshimura², Satoru Kamekura¹, Taku Saito¹, Toshiyuki Ikeda¹, Yosuke Kawasaki¹, Yoshiaki Azuma³, Shiro Ikegawa⁴, Kazuto Hoshi¹, Ung-il Chung¹, Kozo Nakamura¹, Shigeaki Kato² & Hiroshi Kawaguchi¹

Endochondral ossification is an essential process not only for physiological skeletal development and growth, but also for pathological disorders. We recently identified a novel cartilage-specific molecule, carminerin (also known as cystatin 10 and encoded by *Cst10*), which is upregulated in synchrony with cartilage maturation and stimulates the later differentiation of cultured chondrocytes¹. Although carminerin-deficient (*Cst10*^{-/-}) mice developed and grew normally, they had a microscopic decrease in the calcification of hypertrophic chondrocytes at the growth plate. When we created experimental models of pathological endochondral ossification, we observed suppression of chondrocyte calcification during formation of osteoarthritic osteophytes, age-related ectopic ossification and healing of bone fractures in *Cst10*^{-/-} mice. Cultured *Cst10*^{-/-} chondrocytes showed a reduction in calcification with activation of an SRY site in the promoter of the gene encoding nucleotide pyrophosphatase phosphodiesterase 1 (NPP1, encoded by *Enpp1*). Functional NPP1 is required for carminerin deficiency to suppress the pathological endochondral ossifications listed above. Carminerin is the first cartilage-specific protein that contributes to chondrocyte calcification during endochondral ossification under physiological and pathological conditions through the transcriptional inhibition of NPP1.

We generated *Cst10*^{-/-} mice by homologous recombination in mouse embryonic stem cells using a targeting vector to replace exon 1 with the phosphoglycerate kinase-neomycin (PGKneo) cassette (Fig. 1a). Inbreeding of heterozygous *Cst10*^{+/-} mice yielded *Cst10*^{-/-} mice, as determined by Southern blot analysis, at the expected mendelian ratio (Fig. 1b). Neither *Cst10* transcripts nor carminerin protein was detected in the rib cartilage of *Cst10*^{-/-} mice, confirming disruption of the *Cst10* gene (Fig. 1c,d). *Cst10*^{-/-} mice developed and grew similarly to wild-type (*Cst10*^{+/+}) and *Cst10*^{+/-} littermates without abnormalities of major organs (Fig. 1e,f).

Radiological analyses of femurs and tibiae in 8-week-old mice showed that *Cst10*^{-/-} mice experienced decreases in trabecular bone volume mainly at the metaphysis, but not in cortical bone at the diaphysis, as compared to the wild-type littermates (Fig. 2a,b and Supplementary Fig. 1 online). Histological examination of the proximal tibiae indicated a decrease in trabecular bone volume beneath the growth plate of *Cst10*^{-/-} mice (Fig. 2c). Although expression of carminerin was localized mainly in the wild-type hypertrophic chondrocytes, the columnar architecture, expression of type X collagen (Col X) and the entire width of the growth plate were comparable between wild-type and *Cst10*^{-/-} mice, indicating that hypertrophic differentiation of chondrocytes was not affected by the carminerin deficiency (Fig. 2c,d). The width of the calcified layer and the number of calcified chondrocytes, as determined by von Kossa staining, however, were reduced (Fig. 2c,d). Bone volume in the *Cst10*^{-/-} primary spongiosa just beneath the growth plate was significantly reduced ($P < 0.01$), with normal numbers of tartrate-resistant acid phosphatase (TRAP)-positive chondroclasts or osteoclasts, whereas the secondary spongiosa was not affected (Fig. 2c,d and Supplementary Fig. 1). In vertebral bodies that undergo less longitudinal growth by the thinner growth plate than femurs and tibiae, the histomorphometric parameters were comparable between the two genotypes in the growth plate and the primary and secondary spongiosa (Supplementary Fig. 1). These findings indicate that the decrease in trabecular bone adjacent to the growth plate of *Cst10*^{-/-} long bones under physiological conditions resulted primarily from impairment of the calcification of hypertrophic chondrocytes, but not from the abnormality of cartilage resorption by chondroclasts or bone formation by osteoblasts.

We then examined the involvement of carminerin in pathological endochondral ossification by using experimental models involving wild-type and *Cst10*^{-/-} littermates. First, we investigated the role of carminerin in the pathogenesis of osteoarthritis by inducing instability in the mouse knee joint². The joint cartilage destruction was similarly visible at the posterior of the tibiae (Fig. 3a) in both genotypes. The

¹Department of Sensory & Motor System Medicine, Faculty of Medicine, University of Tokyo, Hongo 7-3-1, Bunkyo, Tokyo 113-8655, Japan. ²Institute of Molecular and Cellular Biosciences, University of Tokyo, Yayoi 1-1-1, Bunkyo, Tokyo 113-0032, Japan. ³Teijin Institute for Biomedical Research, Asahigaoka 4-3-2, Hino, Tokyo 191-8512, Japan. ⁴Institute of Physical and Chemical Research (RIKEN), Shirokanedai, Minato, Tokyo 106-8639, Japan. Correspondence should be addressed to H.K. (kawaguchi-ort@h.u-tokyo.ac.jp).

Received 1 January; accepted 7 April; published online 7 May 2006; doi:10.1038/nm1409

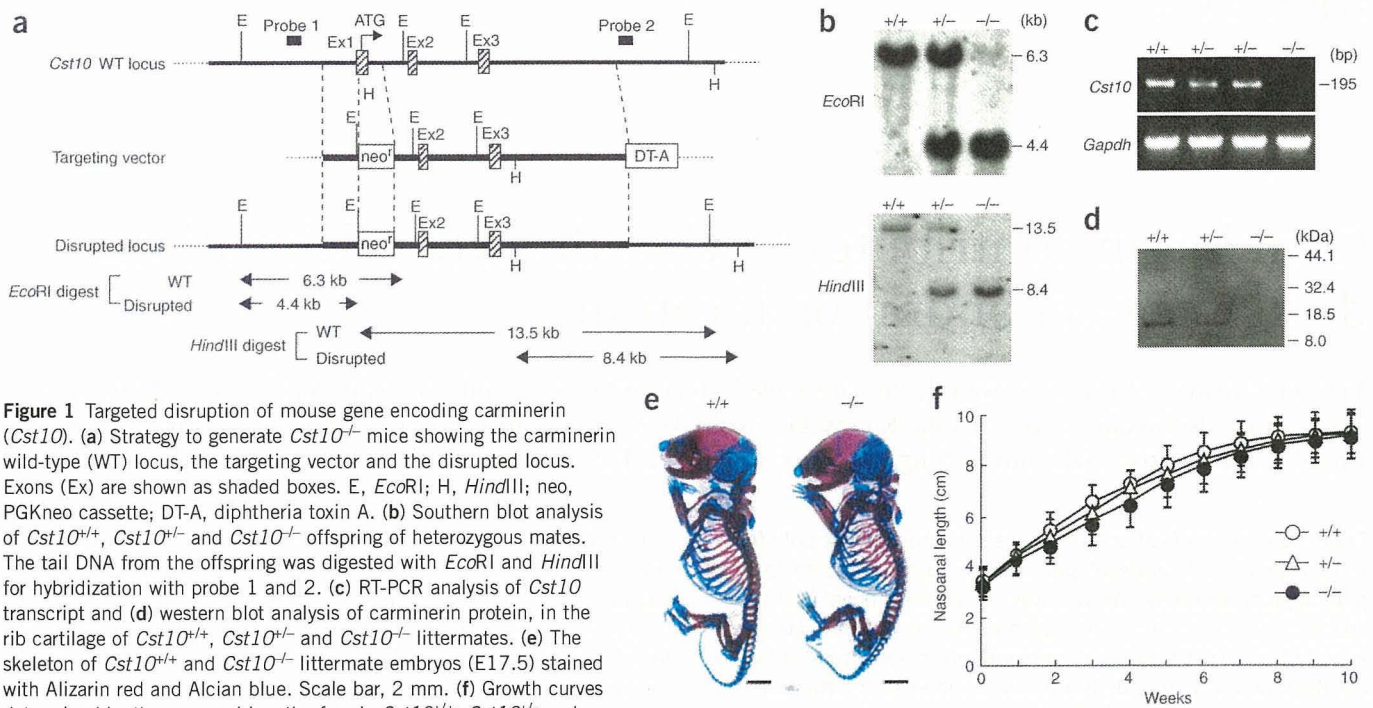


Figure 1 Targeted disruption of mouse gene encoding carminerin (*Cst10*). (a) Strategy to generate *Cst10*^{-/-} mice showing the carminerin wild-type (WT) locus, the targeting vector and the disrupted locus. Exons (Ex) are shown as shaded boxes. E, *EcoRI*; H, *HindIII*; neo, PGKneo cassette; DT-A, diphtheria toxin A. (b) Southern blot analysis of *Cst10*^{+/+}, *Cst10*^{+/-} and *Cst10*^{-/-} offspring of heterozygous mates. The tail DNA from the offspring was digested with *EcoRI* and *HindIII* for hybridization with probe 1 and 2. (c) RT-PCR analysis of *Cst10* transcript and (d) western blot analysis of carminerin protein, in the rib cartilage of *Cst10*^{+/+}, *Cst10*^{+/-} and *Cst10*^{-/-} littermates. (e) The skeleton of *Cst10*^{+/+} and *Cst10*^{-/-} littermate embryos (E17.5) stained with Alizarin red and Alcian blue. Scale bar, 2 mm. (f) Growth curves determined by the nasoanal length of male *Cst10*^{+/+}, *Cst10*^{+/-} and *Cst10*^{-/-} mice. Data are expressed as mean \pm s.e.m. for 15 mice per group. Females also showed similar skeletal development and growth in all genotypes.

carminerin expression was colocalized with Col X in the wild-type hypertrophic chondrocytes adjacent to the osteophyte (Fig. 3b). Although the hypertrophic differentiation of chondrocytes was not affected by the carminerin deficiency (Fig. 3a), osteophyte formation at the posterior of the tibias was significantly decreased (Fig. 3a,c). These findings confirmed by quantification by the Mankin grading score³ and the osteophyte volume (Fig. 3d) indicate that carminerin produced in hypertrophic chondrocytes as a result of mechanical stress contributes to osteophyte formation through chondrocyte calcification, without affecting cartilage destruction or chondrocyte hypertrophy.

Similar findings were observed in ectopic ossification of the patellar ligament and the Achilles tendon with aging (Supplementary Methods online), which was significantly decreased by the carminerin deficiency ($P < 0.05$; Supplementary Fig. 2 online). The colocalization of Col X and carminerin adjacent to the ectopic ossification indicates the involvement of carminerin-expressing hypertrophic chondrocytes in this disorder as well (Supplementary Fig. 2).

We further examined the involvement of carminerin in bone fracture healing at the midshaft of tibias^{4,5}. *Cst10*^{-/-} mice showed a bone gap upon X-ray 3 weeks after the fracture, with substantial formation of cartilaginous callus but impaired calcification, especially at the central area (Fig. 4a). Again, carminerin was expressed in the wild-type chondrocytes adjacent to the calcified callus. The time course of bone mineral content (BMC) showed that calcification in the central one-third portion, but not in the peripheral two-thirds portion, was significantly reduced during the endochondral ossification period (2–7 weeks after fracture) in the *Cst10*^{-/-} callus, although bone union was eventually achieved from the *Cst10*^{-/-} small callus through unaffected bone formation and remodeling thereafter (Fig. 4b). This model also indicates that the carminerin deficiency impaired endochondral ossification, but not intramembranous ossification or osteoblastic bone formation.

The effects of carminerin deficiency on endochondral ossification under the pathological conditions above were more obvious than those under physiological conditions, which showed only a microscopic change. The phenotype of the physiological *Cst10*^{-/-} growth plate was milder than that seen in other disorders such as vitamin A deficiency, which causes not only impaired chondrocyte calcification but also insufficient resorption of unmineralized cartilage by chondroclasts, leading to a suppressed skeletal growth⁶. The difference may be caused by operation of compensatory mechanisms for endochondral ossification, including osteoblastic bone formation and remodeling unaffected by the carminerin deficiency, which are sufficient to compensate for the deficiency under physiological conditions, but not so under pathological conditions.

Carminerin was originally called cystatin 10 because its amino acid sequence contained similarity to the cystatin protein family; however, our examination has not detected legitimate cystatin activity, which inhibits cysteine proteinases (Supplementary Table 1 and Supplementary Methods online). We therefore renamed this protein carminerin after 'cartilage mineralization'. To elucidate the actual mechanism of carminerin action on endochondral ossification, we compared *ex vivo* cultures of chondrocytes isolated from the growth plates of the wild-type and *Cst10*^{-/-} tibias (Supplementary Methods). Although chondrocyte proliferation and differentiation were similar between the two genotypes, chondrocyte calcification was suppressed in the *Cst10*^{-/-} culture (Supplementary Fig. 3 online), indicating a cell-autonomous effect. In contrast, *ex vivo* cultures of primary osteoblasts obtained from wild-type and *Cst10*^{-/-} calvariae confirmed that these cells do not express carminerin, so that there was no difference of bone formation by osteoblasts in this bone type (Supplementary Fig. 3).

As inorganic pyrophosphate (PPi) is known to be a crucial inhibitor of calcification⁷, we compared the expression of a few molecules that

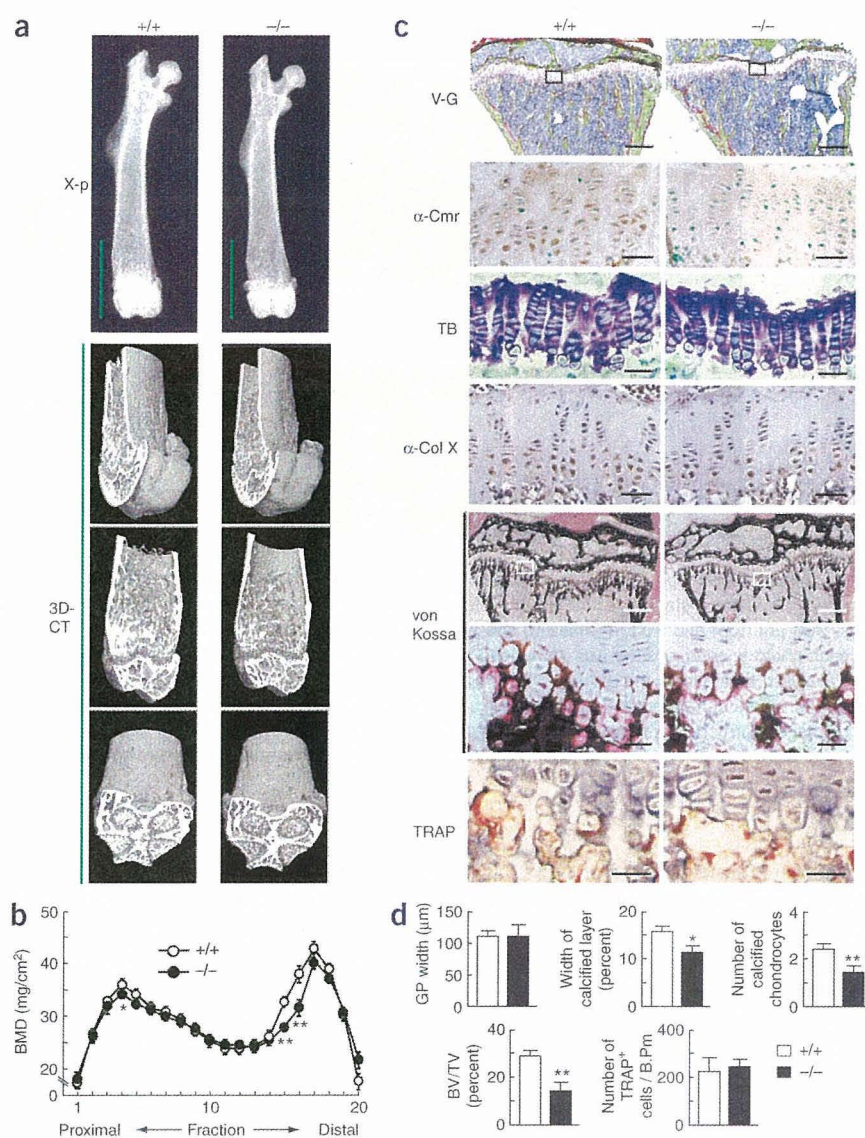


Figure 2 Radiological and histological findings of the long bones in wild-type (*Cst10*^{+/+}) and *Cst10*^{-/-} littermates at 8 weeks of age under physiological conditions. **(a)** Plain X-ray of whole femurs, and three-dimensional computed tomography images of the distal part shown as green lines on the plain X-ray. **(b)** Bone mineral density (BMD) of the 20 equally divided fractions of femurs. **(c)** Histological findings of the proximal tibias. Villanueva-Goldner staining (V-G; scale bar, 200 μ m). Inset boxes indicate the regions of the following three rows: immunostaining with an antibody to carminerin (α -Cmr; scale bar, 20 μ m), toluidine blue staining (TB; scale bar, 20 μ m), immunostaining with an antibody to Col X (α -Col X; scale bar, 20 μ m). von Kossa staining (scale bars, 200 μ m (top) and 20 μ m (bottom)). Inset boxes indicate the regions of the bottom two rows: von Kossa staining and TRAP staining (scale bar, 20 μ m). **(d)** Histomorphometric analyses of the growth plate and primary spongiosa just beneath it. The entire growth plate width (GP width) was measured on the TB sections, and the percent width of calcified layer to the entire growth plate and the number of calcified chondrocytes per column were measured on the von Kossa sections. Bone volume/tissue volume (BV/TV) and the number of TRAP⁺ cells in 100 mm of bone perimeter were measured in the primary spongiosa. Data are expressed as mean \pm s.e.m. for 15 mice per group. **P* < 0.05, ***P* < 0.01 compared to wild-type mice.

control the level of PPI in the cultured growth-plate chondrocytes, including: NPP1, which generates PPI from nucleoside triphosphates using nucleoside triphosphate pyrophosphohydrolase (NTPPPH) activity⁸, tissue-nonspecific alkaline phosphatase (TNAP) which hydrolyzes PPI⁹, and the multiple-pass transmembrane protein ANK, which mediates intracellular-to-extracellular channeling of PPI¹⁰. Among these proteins, the carminerin deficiency upregulated expression of only NPP1, and accordingly, increased NTPPPH activity (**Supplementary Fig. 3**). The reintroduction of carminerin into *Cst10*^{-/-} chondrocytes (*Ax-Cmr*) restored the abnormalities in calcification, expression of NPP1 and NTPPPH activity to those similar to the wild-type culture (**Supplementary Fig. 3**). The promoter activity of an *Enpp1* promoter-luciferase construct (-964 *Enpp1* promoter-Luc) transfected into ATDC5 cells overexpressing carminerin (pCMV-*Cmr*/ATDC5) was lower than cells transfected with mock vector (pCMV/ATDC5; **Supplementary Fig. 3**). Deletion analysis of the *Enpp1* promoter region identified the core responsive element between the -360 and -324 regions, within which an SRY (sex-determining region Y) consensus sequence was predicted. Site-directed mutagenesis to eliminate the SRY site canceled the inhibition of *Enpp1*

transcription by carminerin. Electrophoretic mobility shift assay confirmed specific binding of the SRY region by an oligonucleotide probe with nuclear extracts prepared from pCMV/ATDC5 and pCMV-*Cmr*/ATDC5 cells. Binding by the probe was weaker with the pCMV-*Cmr*/ATDC5 extracts than with the pCMV/ATDC5 extracts (**Supplementary Fig. 3**). As the binding was not detected using the synthetic carminerin protein instead of the nuclear extracts, carminerin itself was shown not to be the direct transcription factor for the SRY region. In contrast, nuclear extracts from the primary *Cst10*^{-/-} growth plate chondrocytes showed stronger binding with the SRY site than those from the wild-type chondrocytes (**Supplementary Fig. 3**). Hence, the transcriptional inhibition of NPP1 expression by carminerin may result, at least partly, from the impaired binding of a transcription factor to the SRY site of the *Enpp1* promoter. Although Sox9, a potent regulator of chondrocyte differentiation^{11,12}, is the most probable transcription factor for this site, we did not observe a supershift of the DNA-protein complex when we added Sox9-specific antibody in the electrophoretic mobility shift assay (data not shown), indicating the involvement of other transcription factors in the regulation of the SRY site. In addition, in our efforts to identify the upstream regulator of NPP1, we did not find substantial regulation of expression or transcription of NPP1 by carminerin through the cytokines interleukin-1 β (IL-1 β), fibroblast growth factor-2 (FGF-2) or transforming growth factor- β (TGF- β), which previously have been reported to regulate NPP1 expression¹³⁻¹⁵ (**Supplementary Fig. 4** online). Thus, further studies to elucidate a more detailed mechanism through which carminerin inhibits transcription of NPP1 will be necessary.

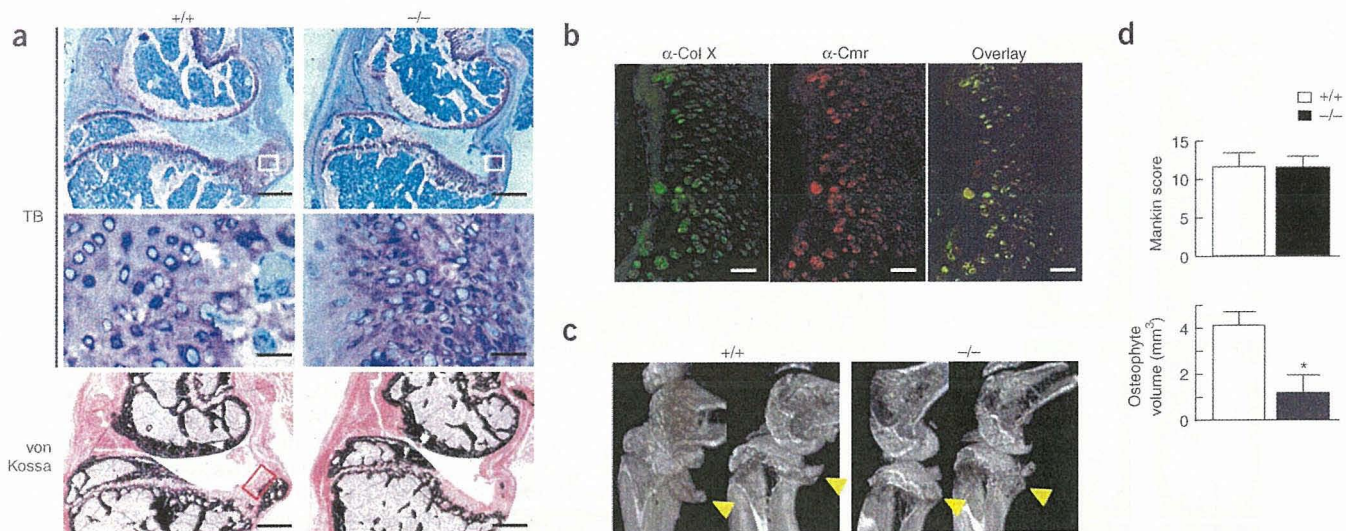


Figure 3 Histological and radiological findings of osteoarthritic joints in wild-type ($Cst10^{+/+}$) and $Cst10^{-/-}$ littermates. (a) Osteoarthritis was induced at the posterior tibias of the knee joint of 8-week-old mice by surgically imposing instability to the joint. Histological features; toluidine blue (TB; inset boxes in the top figures indicate regions shown in middle row; scale bars, 200 μm (top) and 20 μm (middle)) and von Kossa stainings (scale bar, 200 μm) of the sagittal sections of knee joints 10 weeks after surgery (left side of each photo is anterior side). (b) Immunostainings with an antibody to Col X ($\alpha\text{-Col X}$, green), an antibody to carminerin ($\alpha\text{-Cmr}$, red) and the overlay (yellow) analyzed by confocal microscopy in the region indicated in the inset of the image of von Kossa staining of wild-type knee in a. Scale bar, 20 μm . (c) Three-dimensional computed tomography images of the knee joints from the posterolateral projection. Arrowheads indicate osteophytes. (d) Quantification of the cartilage destruction and the osteophyte formation as determined by the Mankin grading score (top) and the osteophyte volume measured on the three-dimensional computed tomography images (bottom), respectively. Data are expressed as mean \pm s.e.m. for ten mice per group. * $P < 0.01$ compared to wild-type mice.

Finally, we carried out *in vitro* fertilization and embryo transfer from $Cst10^{-/-}$ mice and the $Enpp1^{-/-}$ mice, which lack expression of functional NPP1 (ref. 16), and generated four genotypes of mice: $Cst10^{+/+}Enpp1^{+/+}$, $Cst10^{-/-}Enpp1^{+/+}$, $Cst10^{+/+}Enpp1^{-/-}$ and $Cst10^{-/-}Enpp1^{-/-}$. When we used the experimental models, there was no difference in formation of osteoarthritic osteophytes, age-related ectopic ossification or high phosphate-induced auricular ossification

between the NPP1-deficient mice ($Cst10^{+/+}Enpp1^{-/-}$) and the double-deficient mice ($Cst10^{-/-}Enpp1^{-/-}$), confirming that functional NPP1 is essential for suppression of the pathological endochondral ossification by the carminerin deficiency *in vivo* (Supplementary Fig. 5 online).

Our previous *in vitro* study showed that overexpression of carminerin in ATDC5 cells accelerated not only calcification but also

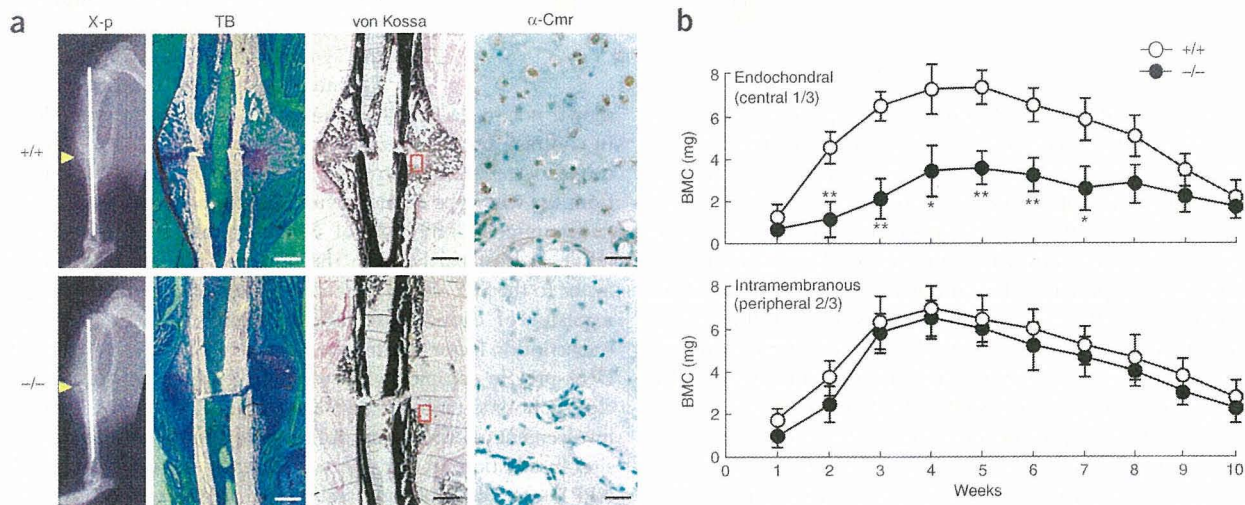


Figure 4 Radiological and histological findings of bone fracture healing in wild-type ($Cst10^{+/+}$) and $Cst10^{-/-}$ littermates. Fracture was produced by a transverse osteotomy that was stabilized with an intramedullary nail at the midshaft of tibias in 8-week-old mice. (a) Plain X-ray, toluidine blue (TB), von Kossa and a carminerin-specific antibody ($\alpha\text{-Cmr}$) immunostainings 3 weeks after fracture. Insets in the image of von Kossa staining indicate regions of immunostaining. Scale bar, 20 μm for immunostaining, and 200 μm for the others. (b) Time course of bone mineral content (BMC) at the fracture callus for 10 weeks after fracture. BMC of the central one-third portion was measured as the endochondral ossification, and BMC of the peripheral two-thirds as the intramembranous ossification. Data are expressed as mean \pm s.e.m. for six mice per time per group. * $P < 0.05$, ** $P < 0.01$ compared to wild-type mice.

hypertrophic differentiation¹. In contrast, the present *in vivo* and *in vitro* studies on deficiency of carminerin showed no abnormality in hypertrophic differentiation of chondrocytes. This discrepancy might owe to the involvement of insulin signaling by way of NPP1 regulation because in addition to the enzymatic function of synthesizing PPI, NPP1 is known to suppress the tyrosine kinase activity of the insulin receptor¹⁷. Considering that our previous ADTC5 cell culture was carried out in the presence of insulin (10 µg/ml), which was essential to induce hypertrophic differentiation¹⁸, overexpression of carminerin might cause suppression of NPP1, which in turn increases sensitivity to insulin and enhances hypertrophic differentiation. The fact that the serum insulin levels in wild-type and *Cst10*^{-/-} mice were similar (0.32 ± 0.08 and 0.35 ± 0.06 ng/ml, respectively; mean ± s.e.m. of five mice per genotype) and were much lower than the *in vitro* concentration, indicates that the regulation of chondrocyte calcification by endogenous carminerin *in vivo* was not mediated by insulin signaling.

Pi has been suggested to be rate limiting for calcification, which may explain why clinical disorders in homeostasis of Pi lead to, for example, rickets, osteomalacia¹⁹ and ectopic calcification²⁰. Considering that carminerin was isolated as a protein that was upregulated by a high-phosphate diet in association with calcification of mouse auricular cartilage, carminerin might partly mediate Pi-induced cartilage calcification. In fact, carminerin deficiency decreased calcification of auricular cartilage in wild-type mice on a high-phosphate diet (Supplementary Fig. 5). Carminerin may therefore be the first cartilage-specific protein that induces chondrocyte calcification during endochondral ossification under physiological and pathological conditions.

METHODS

Generation of *Cst10*^{-/-} mice. We obtained a *Cst10* genomic clone by screening a bacterial artificial chromosome (BAC) library using a BAC PCR screening system (Genome Systems). We used a 120-kb fragment of a BAC clone containing all exons (1–3) of *Cst10* to construct the targeting vector. We constructed the targeting vector to replace exon 1, including the transcription initiation site, by the neomycin-resistance gene. We introduced the linearized targeting vector by electroporation into embryonic stem (ES) cells as previously described²¹, and identified two independent targeted ES cell clones by Southern blot analysis, using 5' (probe 1) and 3' (probe 2) external probes. We generated chimeric males and crossed them with C57BL/6 females, and verified germline transmission by Southern blot analysis. All *Cst10*^{-/-} mice used in this study had been backcrossed for ten generations into the C57BL/6 background. We used RT-PCR to determine the presence of the *Cst10* transcripts. We determined presence of carminerin protein by western blot analysis, as previously described, using a polyclonal antibody to the full-length carminerin protein, which was raised in rabbits using a synthetic peptide of carminerin¹.

Mice conditions. We fed mice a standard rodent diet (CE-2; CLEA Japan) or a high-phosphate diet containing 1.86% phosphorus. In each experiment, we compared littermate wild-type and *Cst10*^{-/-} mice generated from the intercross between heterozygous mice. All experiments were performed on male mice, according to the protocol approved by the Animal Care and Use Committee of the University of Tokyo.

Skeletal preparations. We fixed whole skeletons of wild-type and *Cst10*^{-/-} littermate embryos (E17.5) in 99.5% ethanol, transferred them into acetone and stained them as previously described²¹. We kept specimens in 20% glycerol-1% KOH until skeletons became clearly visible.

Radiological analyses. We took plain radiographs using a soft X-ray apparatus. We measured the bone mineral density (BMD) of the 20 equally divided fractions of the entire femur and bone mineral content (BMC) of the fracture callus with dual energy X-ray absorptiometry using a bone mineral analyzer. We carried out micro-computed tomography scanning using a composite

X-ray analyzer, and reconstructed cross-sectional tomograms of 10 µm thickness at 12 × 12 pixels into a three-dimensional feature by the volume-rendering method; we then measured the ossification volume using a computer. We performed peripheral quantitative computed tomography scans at the metaphysis of 0.2 mm below the proximal growth plate and at the midshaft of tibias.

Histological analyses. For Villanueva-Goldner, toluidine blue and von Kossa stainings, we fixed samples with 70% ethanol, embedded them in glycol methacrylate without decalcification and sectioned them into 3-µm slices. We carried out histomorphometric analyses in the growth plate, primary spongiosa just beneath it (0.3 mm in length) and secondary spongiosa (1.0 mm in length from 0.3 mm below the growth plate) of the proximal tibias and the fifth vertebra using an image analyzer. For double labeling to analyze the dynamic bone remodeling, we subcutaneously injected mice with 8 mg/kg body weight of calcein at 10 d and 3 d before killing. We stained TRAP⁺ cells at pH 5.0 in the presence of L(+)-tartaric acid using naphthol AS-MX phosphate in *N,N*-dimethyl formamide as the substrate. We performed histomorphometric measurements in eight optical fields, according to the American Society for Bone and Mineral Research nomenclature report²², and calculated the averages per mouse. For H&E staining, we perfused mice with 4% buffered paraformaldehyde, decalcified bones with 4.13% EDTA, embedded them in paraffin, and cut them into 6 µm-thick sections. For immunohistochemical analyses, we treated sections as previously described⁴, using polyclonal rabbit antibody to carminerin or Col X (Santa Cruz Biotechnology). For double staining, we treated sections with 1% BSA, incubated them with a mixture of carminerin-specific antibody and mouse monoclonal Col X-specific antibody and with Texas red-conjugated goat antibody to rabbit IgG. They were then reacted with biotin-conjugated antibodies to mouse IgG+IgA+IgM and FITC-streptavidin. The localizations were observed by confocal laser scanning microscopy.

Osteoarthritis model. Eight-week-old mice underwent a microsurgery to produce instability in the knee joints as we reported previously². Mice were killed 10 weeks after surgery, and cartilage destruction was quantified as the Mankin grading score³ of the most severe change among multiple serial toluidine blue sections in each mouse. We measured osteophyte volume with three-dimensional computed tomography as described above.

Fracture model. We produced fracture at the midshaft of tibias of 8-week-old mice as we reported previously^{4,5}. Several mice were killed each week for 10 weeks after the surgery. After the entire callus was longitudinally divided into three equal portions on a bone mineral analyzer image, we measured BMC at the central one-third portion as the endochondral ossification and that at the peripheral two-thirds as the intramembranous ossification. We performed histological analyses 3 weeks after fracture.

Statistical analysis. All data are expressed as mean ± s.e.m. Means of groups were compared by ANOVA and significance of differences was determined by *post hoc* testing using the Bonferroni method.

Note: Supplementary information is available on the Nature Medicine website.

ACKNOWLEDGMENTS

This study was supported by a Grant-in-aid for Scientific Research from the Japanese Ministry of Education, Culture, Sports, Science, and Technology (#14370454), and by the Investigation Committee on the Ossification of Spinal Ligaments, Japanese Ministry of Public Health and Welfare.

COMPETING INTERESTS STATEMENT

The authors declare that they have no competing financial interests.

Published online at <http://www.nature.com/naturemedicine/>

Reprints and permissions information is available online at <http://npg.nature.com/reprintsandpermissions/>

1. Koshizuka, Y. *et al.* Cystatin 10, a novel chondrocyte-specific protein, may promote the last steps of the chondrocyte differentiation pathway. *J. Biol. Chem.* **278**, 48259–48266 (2003).
2. Kamekura, S. *et al.* Osteoarthritis development in novel experimental mouse models induced by knee joint instability. *Osteoarthritis Cartilage* **13**, 632–641 (2005).

3. Mankin, H.J., Johnson, M.E. & Lippiello, L. Biochemical and metabolic abnormalities in articular cartilage from osteoarthritic human hips. III. Distribution and metabolism of amino sugar-containing macromolecules. *J. Bone Joint Surg. Am.* **63**, 131–139 (1981).
4. Shimoaka, T. *et al.* Impairment of bone healing by insulin receptor substrate-1 deficiency. *J. Biol. Chem.* **279**, 15314–15322 (2004).
5. Chikuda, H. *et al.* Cyclic GMP-dependent protein kinase II is a molecular switch from proliferation to hypertrophic differentiation of chondrocytes. *Genes Dev.* **18**, 2418–2429 (2004).
6. Wolbach, S.B. Vitamin-A deficiency and excess in relation to skeletal growth. *J. Bone Joint Surg.* **29**, 171–192 (1947).
7. Terkeltaub, R.A. Inorganic pyrophosphate generation and disposition in pathophysiology. *Am. J. Physiol. Cell Physiol.* **281**, C1–C11 (2001).
8. Bollen, M., Gijsbers, R., Ceulemans, H., Stalmans, W. & Stefan, C. Nucleotide pyrophosphatases/phosphodiesterases on the move. *Crit. Rev. Biochem. Mol. Biol.* **35**, 393–432 (2000).
9. Balcerzak, M. *et al.* The roles of annexins and alkaline phosphatase in mineralization process. *Acta Biochim. Pol.* **50**, 1019–1038 (2003).
10. Ryan, L.M. The ank gene story. *Arthritis Res.* **3**, 77–79 (2001).
11. de Crombrugge, B., Lefebvre, V. & Nakashima, K. Regulatory mechanisms in the pathways of cartilage and bone formation. *Curr. Opin. Cell Biol.* **13**, 721–727 (2001).
12. Akiyama, H., Chaboissier, M.C., Martin, J.F., Schedl, A. & de Crombrugge, B. The transcription factor Sox9 has essential roles in successive steps of the chondrocyte differentiation pathway and is required for expression of Sox5 and Sox6. *Genes Dev.* **16**, 2813–2828 (2002).
13. Lotz, M. *et al.* Interleukin 1 beta suppresses transforming growth factor-induced inorganic pyrophosphate (PPI) production and expression of the PPI-generating enzyme PC-1 in human chondrocytes. *Proc. Natl. Acad. Sci. USA* **92**, 10364–10368 (1995).
14. Solan, J.L., Deftos, L.J., Goding, J.W. & Terkeltaub, R.A. Expression of the nucleoside triphosphate pyrophosphohydrolase PC-1 is induced by basic fibroblast growth factor (bFGF) and modulated by activation of the protein kinase A and C pathways in osteoblast-like osteosarcoma cells. *J. Bone Miner. Res.* **11**, 183–192 (1996).
15. Oyajobi, B.O., Caswell, A.M. & Russell, R.G. Transforming growth factor beta increases ecto-nucleoside triphosphate pyrophosphatase activity of human bone-derived cells. *J. Bone Miner. Res.* **9**, 99–109 (1994).
16. Okawa, A. *et al.* Mutation in Npps in a mouse model of ossification of the posterior longitudinal ligament of the spine. *Nat. Genet.* **19**, 271–273 (1998).
17. Goldfine, I.D., Maddux, B.A., Youngren, J.F., Trischitta, V. & Frittitta, L. Role of PC-1 in the etiology of insulin resistance. *Ann. NY Acad. Sci.* **892**, 204–222 (1999).
18. Shukunami, C. *et al.* Chondrogenic differentiation of clonal mouse embryonic cell line ATDC5 *in vitro*: differentiation-dependent gene expression of parathyroid hormone (PTH)/PTH-related peptide receptor. *J. Cell Biol.* **133**, 457–468 (1996).
19. Laroche, M. Phosphate, the renal tubule, and the musculoskeletal system. *Joint Bone Spine* **68**, 211–215 (2001).
20. Jono, S. *et al.* Phosphate regulation of vascular smooth muscle cell calcification. *Circ. Res.* **87**, E10–E17 (2000).
21. Nakamichi, Y. *et al.* Chondromodulin I is a bone remodeling factor. *Mol. Cell. Biol.* **23**, 636–644 (2003).
22. Parfitt, A.M. *et al.* Bone histomorphometry: standardization of nomenclature, symbols, and units. Report of the ASBMR Histomorphometry Nomenclature Committee. *J. Bone Miner. Res.* **2**, 595–610 (1987).

Topical vitamin D3 and low-calcemic analogs induce thymic stromal lymphopoietin in mouse keratinocytes and trigger an atopic dermatitis

Mei Li*, Pierre Hener*, Zhikun Zhang*, Shigeaki Kato†, Daniel Metzger*, and Pierre Chambon**

*Institut de Génétique et de Biologie Moléculaire et Cellulaire and Institut Clinique de la Souris, BP10142, 67404 Illkirch Cedex, France; and †Institute of Molecular and Cellular Biosciences, University of Tokyo, 1-1-1 Yayoi, Bunkyo-ku, Tokyo 113-0032, Japan

Contributed by Pierre Chambon, June 5, 2006

We have demonstrated that cytokine thymic stromal lymphopoietin (TSLP), whose expression is rapidly induced upon keratinocyte-selective ablation of retinoid X receptors (RXRs) α and β in the mouse (RXR $\alpha\beta^{ep-/-}$ mice), plays a key role in initiating a skin and systemic atopic dermatitis-like phenotype. We show here that topical application of the physiologically active ligand [1 α ,25-(OH) $_2$ D $_3$; calcitriol] of the vitamin D receptor, or of its low-calcemic analog MC903 (calcipotriol; Dovonex), induces TSLP expression in epidermal keratinocytes, which results in an atopic dermatitis-like syndrome mimicking that seen in RXR $\alpha\beta^{ep-/-}$ mutants and transgenic mice overexpressing TSLP in keratinocytes. Furthermore, topical application of retinoic acid receptor RAR γ -selective agonist BMS961 also induces TSLP expression either on its own or synergistically with 1 α ,25-(OH) $_2$ D $_3$. Our data demonstrate that RXR/vitamin D receptor and RXR/retinoic acid receptor- γ heterodimers and their ligands cell-autonomously control the expression of TSLP in epidermal keratinocytes of the mouse. We propose molecular mechanisms through which vitamin D3 and retinoic acid signalings could be involved in the pathogenesis of atopic diseases.

retinoic acid | vitamin D receptor | retinoid X receptor |
retinoic acid receptor | skin

Nuclear receptors (NRs) belong to a superfamily of ligand-dependent transcriptional regulators (1, 2). Within this superfamily, retinoid X receptors (RXRs) α , β , and γ play a key role through heterodimerization with some 15 NR partners, e.g., retinoic acid receptors (RARs), vitamin D receptor (VDR), peroxisome proliferator-activated receptors, and liver X receptors (1, 2). We reported (3) that selective ablation of RXR α and RXR β in adult mouse epidermal keratinocytes (RXR $\alpha\beta^{ep-/-}$ mice) triggers a skin and systemic syndrome similar to human atopic dermatitis (AD), a chronic skin inflammatory disease with a strong genetic component that affects children (10–20%) and adults (1–3%) (4). These mice exhibit the major features of the human AD syndrome that include (i) skin eczematous-like lesions with xerosis and pruritus, associated with a skin inflammatory infiltrate mainly composed of CD4 $^+$ T helper (Th) type 2 cells, dendritic cells, eosinophils, and mast cells and (ii) systemic abnormalities, including elevated serum IgE and IgG levels and blood and tissue eosinophilia.

We found that expression of the cytokine thymic stromal lymphopoietin (TSLP), known to be produced in epidermal keratinocytes of AD patients (5), is rapidly induced in keratinocytes of RXR $\alpha\beta^{ep-/-}$ mice. Furthermore, we showed that K14-TSLP transgenic mice overexpressing TSLP in keratinocytes exhibit an AD-like phenotype similar to that of RXR $\alpha\beta^{ep-/-}$ mice (3), demonstrating that TSLP can act as an initiating cytokine at the top of a chain of immunological events that lead to an AD-like phenotype, in keeping with other recent studies on mouse models of human allergic inflammatory diseases (asthma and AD) (6–9).

We suggested that up-regulation of keratinocytic TSLP expression upon RXR α and β ablation could be due to the relief of a transcriptional repression mediated by RXR/NR heterodimers (3).

This study was aimed at revealing the identity of the possible NR partner(s) of RXR α and RXR β .

Results

Topical Application of 1 α ,25-(OH) $_2$ D $_3$ or Its Low-Calcemic Analog MC903 Activates TSLP Expression in Epidermal Keratinocytes. Because RXR/NR heterodimers in which an agonistic ligand is not bound to the NR partner can act as transcriptional repressors (10), we examined whether TSLP expression could be induced by NR agonists. Four nanomoles of ligands were topically applied to whole ears of WT mice for 4 consecutive days (days 1–4), and TSLP RNA levels were determined on day 5. Application of 1 α ,25-(OH) $_2$ D $_3$ (the physiologically active vitamin D3) led to a dramatic increase (>300-fold) in TSLP transcripts at day 5, whereas they were modestly but significantly increased (5-fold) upon application of a RAR γ -selective agonist (BMS961) (11) (Fig. 1*a*). In contrast, agonists for RXRs (BMS649), proliferator-activated receptor (PPAR) α (fenofibrate), PPAR β (GW501516), PPAR γ (rosiglitazone), and liver X-activated receptors (25-hydroxycholesterol) had no effect on TSLP expression (Fig. 1*a*).

Because, at this dose, 1 α ,25-(OH) $_2$ D $_3$ application resulted in hypercalcemia and death of the mice, we applied its analog MC903 (calcipotriol; Dovonex) (12) that exhibits a low-calcemic activity and is used for psoriasis treatment (13). MC903 and ethanol (vehicle) were applied to WT mouse right and left ears, respectively. Two shaved areas (1 cm 2 each) of dorsal skin were also treated with MC903 or ethanol. One day after the first application (day 2), TSLP RNA levels were increased in right ears and further increased on days 3 and 4, whereas no increase occurred in left ears (Fig. 1*b Left*). Transcripts of *CYP24A1*, a 1 α ,25-(OH) $_2$ D $_3$ -inducible gene (14), were increased upon MC903 application, as expected (Fig. 1*b, Right*). TSLP RNA was also increased in MC903-treated dorsal skin (Fig. 1*c*), and serum TSLP levels were increased at days 2–4, whereas undetectable at day 0 (before treatment) (Fig. 1*d*). Increasing doses of MC903 (0.4, 1, or 4 nmol per ear) led to a dose-dependent increase of TSLP transcripts, which was similarly observed with other low-calcemic analogs of 1 α ,25-(OH) $_2$ D $_3$, including EB1089 and KH1060 (12, 15) (data not shown).

To examine whether MC903-induced expression of TSLP was skin-restricted, various other organs were analyzed at day 5. No increase in TSLP transcripts was observed in these organs (Fig. 1*e*). Immunohistochemistry (IHC) did not reveal TSLP expression in epidermis or dermis of ethanol-treated ear and dorsal skin, whereas it was readily detected at day 4 upon MC903 treatment (Fig. 1*f*; ear skin, *Upper*; dorsal skin, *Lower*). Double IHC for TSLP and keratin 1 (K1), a suprabasal keratinocyte marker, showed that TSLP was

Conflict of interest statement: No conflicts declared.

Abbreviations: AD, atopic dermatitis; CT, control; IHC, immunohistochemistry; NR, nuclear receptor; RA, retinoic acid; RAG1, recombination activating gene 1; RAR, RA receptor; RXR, retinoid X receptor; Th, T helper; TLR, Toll-like receptor; TSLP, thymic stromal lymphopoietin; VDR, vitamin D receptor.

†To whom correspondence should be addressed. E-mail: chambon@igbmc.u-strasbg.fr.

© 2006 by The National Academy of Sciences of the USA

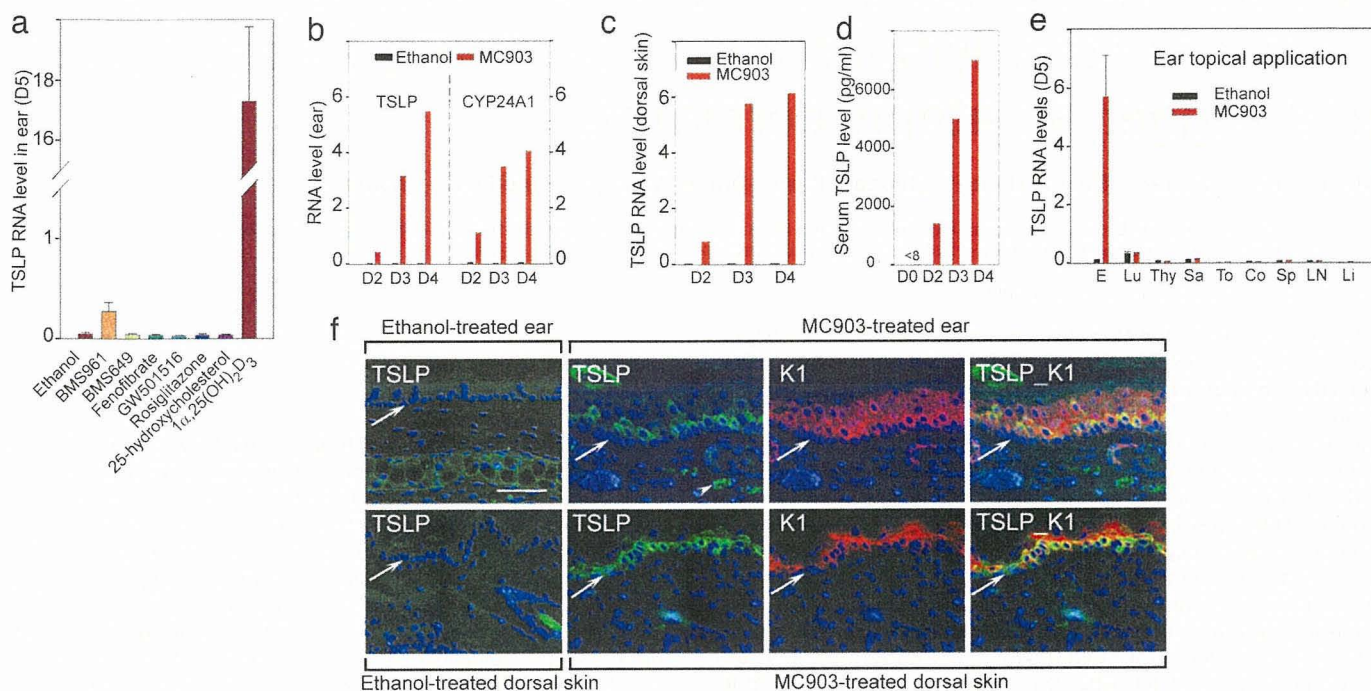


Fig. 1. Skin topical application of $1\alpha,25-(OH)_2D_3$ and MC903 activates TSLP expression in epidermal keratinocytes. (a) TSLP RNA at day 5 in ears topically treated with NR agonists (4 nmol). (b–e) Induction of TSLP expression is a rapid and local skin effect. TSLP and CYP24A1 RNA levels in an ethanol-treated left ear and MC903-treated right ear (b), TSLP RNA levels in ethanol-treated and MC903-treated dorsal skin at days 2, 3, and 4 (c), and increased serum TSLP levels at days 2, 3, and 4 (d), in contrast to undetectable level (<8 pg/ml) at day 0 (before treatment). Data are representative of three independent experiments. D, day. (e) TSLP RNA levels at day 5 in ear (E), lung (Lu), thymus (Thy), salivary gland (Sa), tongue (To), colon (Co), spleen (Sp), lymph node (LN), and liver (Li) of mice topically treated by ethanol or MC903 on ears. (f) IHC of TSLP (green) at day 4 in sections of ear (Upper) and dorsal skin (Lower) topically treated with ethanol or MC903. The same sections from MC903-treated skin were stained with keratin 1 antibody (K1, red), and overlaid images of TSLP and K1 staining are shown, as indicated. Blue corresponds to DAPI staining of nuclei. The white arrowhead points to autofluorescent erythrocytes, and white arrows point to the dermal/epidermal junction. (Scale bar, 50 μ m.)

mainly located in these keratinocytes of both MC903-treated ear and dorsal skin, whereas it could also be detected at a lower level in basal keratinocytes (expressing keratin 14) (Fig. 1f, and data not shown).

Topical Application of MC903 Triggers an AD-Like Syndrome. Because TSLP expression appears to be critically involved in the initiation of AD-like dermatitis in the mouse (3, 8), we investigated whether a MC903 long-term treatment could induce an AD-like phenotype. MC903 (4 nmol) was applied daily for 16 days to ears of WT mice. No hypercalcemia or overall health impairment and weight loss was observed. Ethanol application did not cause any change in ear appearance, whereas reddening and swelling that worsened with time were observed from day 5 on MC903-treated ears (data not shown). At day 17, these ears were red, scaly, swollen, and crusted (Fig. 2, compare *a* and *b*), and frequent ear scratching (data not shown) suggested a pruritus. Histological analysis revealed epidermal hyperplasia and a heavy dermal cell infiltrate, in which numerous eosinophils were easily identified upon hematoxylin/eosin-staining (Fig. 2d and *Inset*). Their identity was confirmed with Luna's staining (data not shown). In contrast, no eosinophils were found in ethanol-treated ears (Fig. 2c). IHC with an anti-GR1 antibody (recognizing granulocytes and monocytes) revealed a large number of positive cells in dermis, of which eosinophils, but not neutrophils, were a major component (Fig. 2f and data not shown). Numerous T lymphocytes ($CD3^+$) were observed in MC903-treated dermis (Fig. 2h), whereas only a few resident T lymphocytes could be detected in ethanol-treated ears (Fig. 2g). Most of the infiltrated T cells were $CD4^+$ helper T cells (Fig. 2j), and only a few $CD8^+$ cytotoxic T cells were found (Fig. 2l). A large

increase in $CD11c^+$ dermal dendritic cells was also observed in MC903-treated ears (Fig. 2m and *n*), whereas mast cells were 4-fold increased in the dermis (Fig. 2o and *p* and data not shown).

Because topical application of $1\alpha,25-(OH)_2D_3$ at a dose of 4 nmol per ear resulted in mouse death within 7 days, WT mice were thus treated every other day at a dose of 0.25 nmol per ear, to examine whether the treatment would result in a skin inflammation similar to that generated with MC903. At this dose, TSLP expression was significantly induced at day 18, and an inflammatory infiltrate comprising $CD4^+$ T lymphocytes, dendritic cells, eosinophils, and mast cells could also be observed (data not shown).

Taken together, these data indicated that the inflammatory cell infiltrate observed in skin of MC903- and $1\alpha,25-(OH)_2D_3$ -treated ears had the characteristics of an AD-like skin inflammation (3). This finding was fully supported by analysis of cytokines expressed in MC903-treated ears. At day 16, TSLP transcripts were markedly increased (Fig. 2q), and Th2-type cytokine transcripts (IL-4, -5, -13, -31, -10, and -6) (3) were all significantly increased (Fig. 2q). Expression of the Th1-type cytokine IFN- γ was also enhanced, whereas that of TNF- β , another Th1-type cytokine, was unchanged. Importantly, this cytokine profile, which is essentially that of a Th2-type inflammation, was similar to those observed in skins of $RXR\alpha\beta^{cp-/-}$ and K14-TSLP transgenic mice (3), indicating that the increase of these cytokines was most probably due to enhanced TSLP production in keratinocytes.

Systemic abnormalities, including elevated serum IgE and IgG levels, associated with blood and tissue eosinophilia, have been observed in $RXR\alpha\beta^{cp-/-}$ and K14-TSLP mice, exhibiting similarities to those observed in AD patients (3). Serum IgE and IgG levels were increased in mice to which MC903 was topically applied for 16

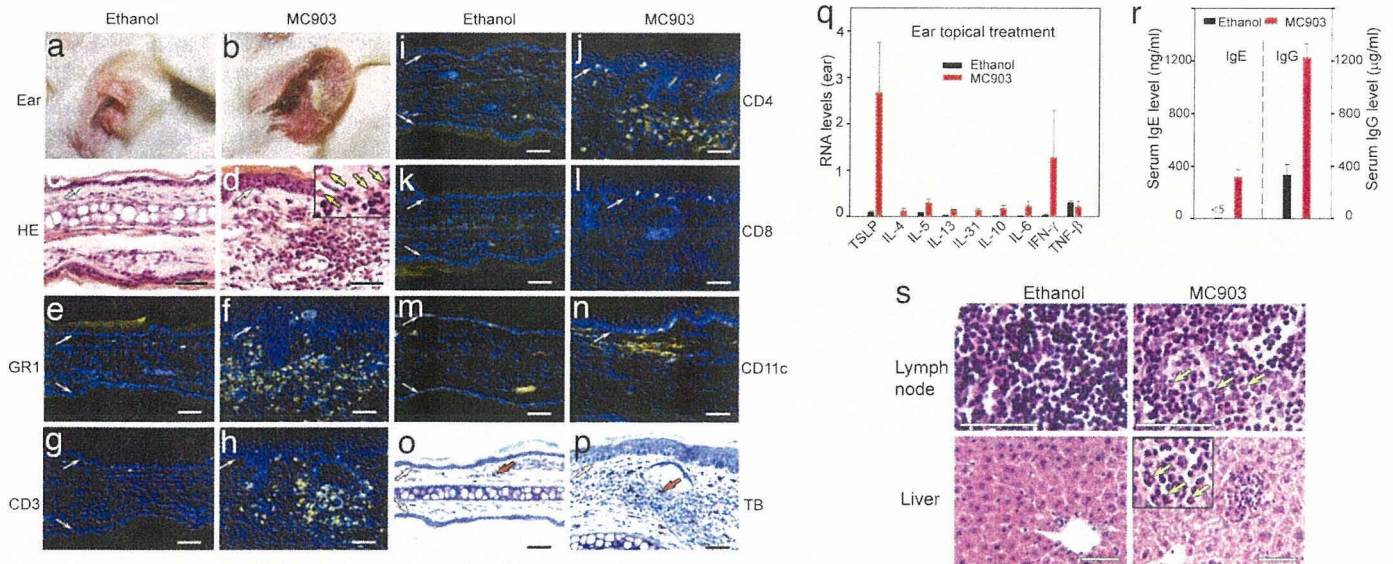


Fig. 2. Topical treatment with MC903 triggers an AD-like skin inflammation. (a and b) Appearance of ethanol- and MC903-treated ears at day 17. (c and d) Hematoxylin and eosin-stained ear sections of ethanol- and MC903-treated mice at day 17. Eosinophils displaying cytoplasmic red staining are indicated by yellow arrows in *d Inset*. (e–n) IHC performed on ear sections from ethanol- or MC903-treated mice at day 17, with antibodies against GR1 (e and f), CD3 (g and h), CD4 (i and j), CD8 (k and l), and CD11c (m and n). Yellow corresponds to staining of antibodies, whereas blue corresponds to DAPI staining of nuclei. (o and p) Toluidin blue (TB) staining of ear sections. Red arrows point to one of the mast cells with intense blue in the dermis. White arrows in c–p point to the dermal/epidermal junction. (q) Cytokine RNA levels in ethanol- and MC903-treated ears at day 17. (r) Serum IgE and IgG levels of ethanol- and MC903-treated mice at day 17. (s) Hematoxylin and eosin-stained sections of ear-draining lymph node and liver of ethanol- and MC903-treated mice at day 17. Yellow arrows point to three of many eosinophils (red cytoplasmic staining) in sections of lymph node and liver of MC903-treated mice. (Scale bars, 50 μ m.)

days on ears (Fig. 2r). Moreover, at day 16, MC903-treated mice exhibited an increased number of eosinophils in ear-draining lymph nodes, liver, and spleen (Fig. 2s and data not shown). Differential blood cell counts also revealed a marked increase in eosinophils in MC903-treated mice (693 ± 220 cells per μ l, versus 204 ± 134 cells per μ l in ethanol-treated mice). Thus, MC903 topical application leads to a skin and systemic phenotype mimicking that of human AD.

Both Keratinocytic VDR and RXR Are Required for Induction of TSLP Expression and Generation of an AD-Like Skin Inflammation Upon MC903 Treatment. To investigate whether the MC903-induced TSLP expression and appearance of an AD-like skin inflammation were mediated through VDR, MC903 was topically applied on ears of “floxed” VDR control (CT) mice (VDR^{L2/L2} mice in which both VDR alleles bear LoxP sites) and of their VDR^{ep-/-} littermates [K14-Cre^(tg/0)/VDR^{L2/L2} mice] in which the VDR alleles are selectively ablated in keratinocytes (ref. 16 and our unpublished data). At day 17 of MC903 treatment, an inflammation was obvious on ears of VDR CT mice, whereas VDR^{ep-/-} ears did not show any sign of inflammation (Fig. 3a and b). Accordingly, a massive dermal infiltrate of inflammatory cells, including eosinophils, CD4⁺ Th cells, dendritic cells, and mast cells was detected in ear sections of MC903-treated VDR CT (Fig. 3c and data not shown) but not in those of VDR^{ep-/-} mice (Fig. 3d). Similarly, no AD-like skin inflammation was developed upon topical MC903 treatment of VDR^{-/-} (germ-line knockout) mice (17) (data not shown).

TSLP expression was strongly induced in MC903-treated skin of VDR CT mice (Fig. 3e, lanes 1 and 2) but not at all in MC903-treated skin of VDR^{-/-} mice (lanes 5 and 6), whereas it was weakly increased in MC903-treated skin of VDR^{ep-/-} mutants (lanes 3 and 4). This latter increase may reflect a faint response to MC903 in nonkeratinocytic skin cells. In any event, our data clearly demonstrated that induction of TSLP expression in keratinocytes upon MC903 application is a VDR-dependent cell-autonomous event.

To examine whether the effect of MC903 was transduced through RXR/VDR heterodimers, ears of RXR $\alpha\beta$ ^{ep-/-} mice (3) as well as

their control littermates (RXR $\alpha\beta$ CT) were topically treated with MC903 (Fig. 3f). As expected (3), selective RXR $\alpha\beta$ ablation in keratinocytes of adult mice led to increased TSLP expression (lanes 1 and 3). However, the further induction of TSLP by MC903 was severely reduced in RXR $\alpha\beta$ ^{ep-/-} skin (lanes 2 and 4), indicating an essential function of keratinocytic RXRs in TSLP induction by VDR agonists, most probably reflecting the involvement of RXR/VDR heterodimers.

VDR and RAR γ Agonistic Ligands Synergize to Induce Skin TSLP Expression. Although much less potent than that of a VDR agonist, application of a RAR γ -selective agonist (BMS961) on mouse ear skin led to significant increase of TSLP transcripts (Fig. 1a), and topical application of retinoic acid (RA) resulted in a similar induction (data not shown). To examine whether VDR and RAR γ agonists could synergize in up-regulating TSLP expression, WT mouse ears were topically treated for 3 days with ethanol, BMS961 (4 nmol), a limiting dose of 1 α ,25-(OH)₂D₃ (0.4 nmol), or a combination of the two ligands. Ear TSLP transcripts and serum TSLP were determined at day 4. A clear synergism was observed between the effects of BMS961 and 1 α ,25-(OH)₂D₃ (Fig. 4a), indicating a synergistic involvement of RAR- and VDR-mediated events in transcriptional activation of TSLP expression.

TSLP Production and Skin Inflammation Induced by MC903 Are T and B Lymphocyte-Independent. As a direct effect of 1 α ,25-(OH)₂D₃ on naïve CD4⁺ T cells may enhance the development of Th2 cells (18), we investigated whether CD4⁺ T cells are required for development and progression of the active vitamin D₃-induced AD-like phenotype. Ethanol or MC903 was applied on ears of RAG1^{-/-} mice, which are devoid of mature B and T lymphocytes (19). As observed in WT mice, keratinocytic TSLP expression at day 4 was induced in MC903-treated, but not in ethanol-treated, RAG1^{-/-} mice (see Fig. 6a, b, and k, which is published as supporting information on the PNAS web site). At day 16, MC903-treated RAG1^{-/-} mice exhibited thickened and scaly red ears (Fig. 6d), associated with a dermal cell infiltrate and an epidermal hyperplasia (Fig. 6f),

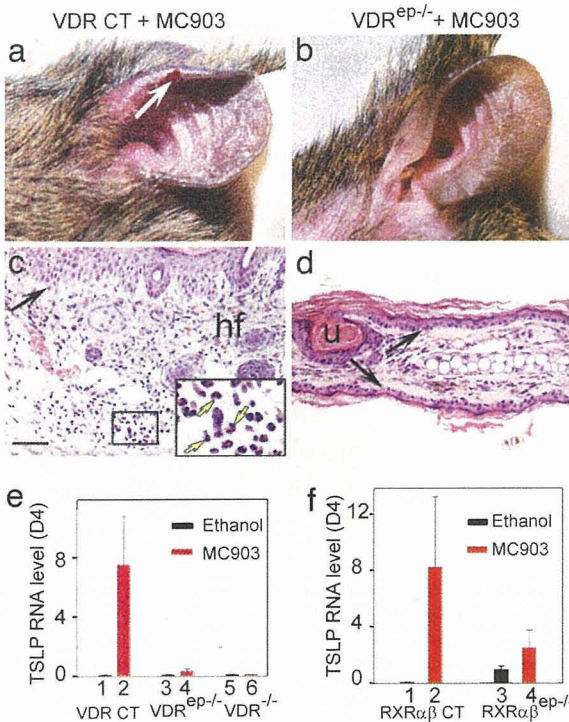


Fig. 3. Keratinocytic VDR and RXR are required for generation of an AD-like skin inflammation and induction of TSLP expression upon MC903 treatment. Appearance of MC903-treated ears of VDR CT (a) and VDR^{ep-/-} mice (b) at day 17. White arrow in a points to lesioned skin. (c and d) Hematoxylin and eosin-stained ear sections. Yellow arrows in c inset point to three of many eosinophils (red cytoplasmic staining) in MC903-treated CT skin. Black arrows point to dermal/epidermal junction, hf, hair follicle; u, utriculi (resulting from hair follicle degeneration in VDR^{ep-/-} mice). (Scale bar, 50 μ m.) (e) TSLP RNA levels at day 4 in ethanol- and MC903-treated ears of VDR CT (lanes 1 and 2), VDR^{ep-/-} (lanes 3 and 4), and VDR^{-/-} (lanes 5 and 6) mice. (f) TSLP RNA levels at day 4 in ethanol- and MC903-treated ears of RXR $\alpha\beta$ CT (lanes 1 and 2) and RXR $\alpha\beta$ ^{ep-/-} (lanes 3 and 4) mice.

whereas ethanol-treated RAG1^{-/-} ears had a normal appearance (Fig. 6c and e). As expected, lymphocytes were absent in RAG1^{-/-} skin sections (data not shown). However, we detected an increased number of infiltrated eosinophils (Fig. 6f vs. e), mast cells (Fig. 6h vs. g), and dermal dendritic cells (Fig. 6j vs. i) in MC903-treated RAG1^{-/-} skin. Thus, enhancement of TSLP expression and generation of a skin inflammation upon MC903-treatment do not require the presence of mature B and T lymphocytes.

Moreover, whereas transcripts of Th2-type cytokines IL-5, -13, and -31 were not increased in MC903-treated RAG1^{-/-} skin (as compared with ethanol treatment), an increase in transcripts of other Th2-type cytokines IL-4, -6, and -10 was observed (Fig. 6k), indicating that these cytokines can be produced by nonlymphocytic cells upon topical MC903 treatment. A marginal increase of IFN- γ was also observed (Fig. 6k). Eosinophilia in blood and some tissues (e.g., ear-associated lymph nodes, liver, and spleen) was also observed in MC903-treated RAG1^{-/-} mice (data not shown), whereas no immunoglobulins could be detected in sera (data not shown), indicating that increased levels of IgE or IgG were not indispensable for generating an AD-like syndrome.

Discussion

Selective ablation of both RXR α and - β in mouse skin keratinocytes results in a marked increase of TSLP expression that leads to the development of an AD-like phenotype (3). Because (i) putative NR response elements are present in mouse and human (20) TSLP promoters (see Fig. 4b and c); (ii) TSLP repression did not require

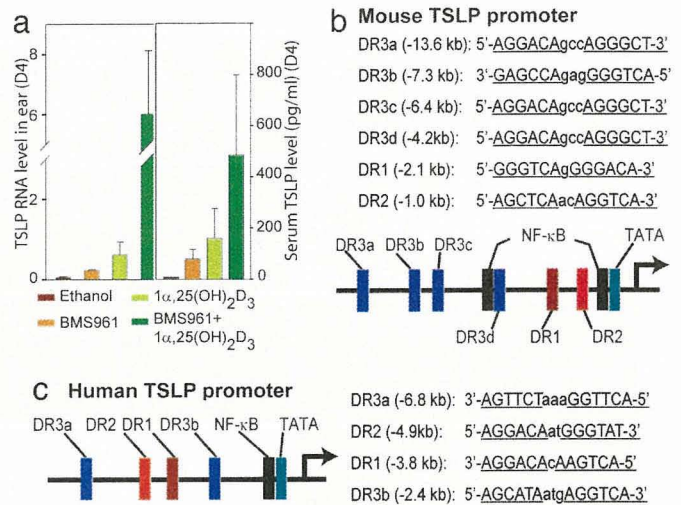


Fig. 4. Agonist-liganded VDR and RXR γ synergistically induce TSLP expression. (a) Mouse ears were treated with ethanol, BMS961 (4 nmol), 1 α ,25-(OH) $_2$ D $_3$ (0.4 nm), or BMS961 (4 nmol) plus 1 α ,25-(OH) $_2$ D $_3$ (0.4 nmol), as indicated. TSLP RNA levels in the ears (Left) and serum TSLP levels (Right) were measured at day 4. (b) Putative VDREs (DR3) and RAREs (DR2 and DR1) upstream of the mouse TSLP promoter. (c) Putative VDREs (DR3) and RAREs (DR2 and DR1) upstream of the human TSLP promoter.

the AF-2 activation function of RXRs; and (iii) TSLP induction could not be triggered by an RXR agonist (Fig. 1a), we proposed (3) that this TSLP overexpression could reflect the relief of a transcriptional repression exerted by nonpermissive RXR/NR(s) heterodimers (21) in which the NR partner is unliganded. We demonstrate here that RXR $\alpha(\beta)$ /VDR heterodimers are such heterodimers, because topical treatment of mouse skin with 1 α ,25-(OH) $_2$ D $_3$ or its low-calcemic analogs strongly induces TSLP expression in skin keratinocytes and triggers a skin and systemic AD-like syndrome mimicking that observed in RXR $\alpha\beta$ ^{ep-/-} mutant and K14-TSLP transgenic mice (3). Moreover, the induction of TSLP by active vitamin D $_3$ is a cell-autonomous event, because it is abolished upon keratinocyte-selective ablation of either VDR or RXR α and - β . We also show that, although less efficiently than RXR $\alpha(\beta)$ /VDR heterodimers, RXR $\alpha(\beta)$ /RAR γ heterodimers liganded with RA or the RAR γ -selective agonist BMS961, also mediate induction of TSLP expression but to a level too low to trigger, on its own, an overt AD-like phenotype. In keeping with these data, TSLP expression can be induced by 1 α ,25-(OH) $_2$ D $_3$ and RA in a mouse epithelial tumor cell line (C1271, derived from a mammary carcinoma) (our unpublished data); TSLP was also shown to be induced by 1 α ,25-(OH) $_2$ D $_3$ in a human epithelial tumor cell line (SCC25, derived from a tongue squamous cell carcinoma) (20). Furthermore, that agonists of VDR and RAR γ could induce TSLP expression either on their own or synergistically indicates that the corresponding RXR heterodimers bind to distinct cognate response elements. In this respect, it is noteworthy that both mouse and human TSLP promoter regions contain putative response elements (Fig. 4b and c) that may bind RXR/VDR heterodimers [vitamin D response element (VDRE):DR3] or RXR/RAR heterodimers [RA response element (RARE):DR2 and DR1] (22).

Based on this evidence, we propose a model accounting for the modulation of TSLP promoter activity by RXR $\alpha(\beta)$ /VDR and RXR $\alpha(\beta)$ /RAR γ heterodimers (schematized in Fig. 5). The promoter region of mouse and human TSLP genes includes a TATA box element and proximal elements (e.g., NF- κ B-binding sites) (the basal promoter) as well as putative VDREs and RAREs (Fig. 4b and c). Because, under homeostatic conditions *in vivo*, there is no RA and very little, if any, active vitamin D $_3$ (see below) in epidermal keratinocytes, the TSLP promoter basal activity is si-

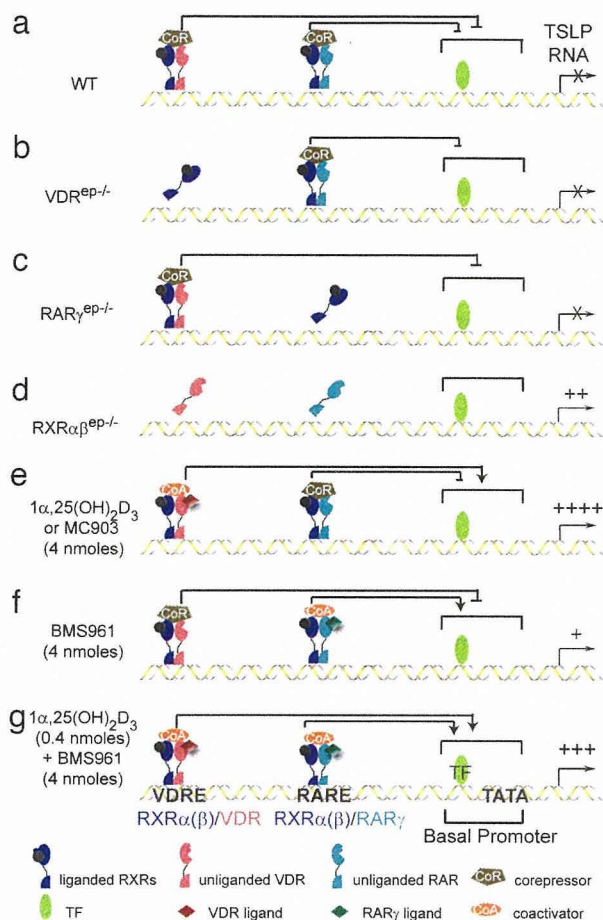


Fig. 5. Schematic model of RXR $\alpha(\beta)$ /VDR- and RXR $\alpha(\beta)$ /RAR γ -mediated regulation of TSLP expression in mouse keratinocytes (see *Discussion*). As concluded from our study (25), keratinocytic RXRs are shown bound to a non-RA-agonistic ligand.

lenced by unliganded RXR $\alpha(\beta)$ /VDR and RXR $\alpha(\beta)$ /RAR γ heterodimers associated with corepressors (10) (Fig. 5a). This repression can be efficiently exerted by either RXR $\alpha(\beta)$ /VDR or RXR $\alpha(\beta)$ /RAR γ heterodimers, because it cannot be relieved by ablation of either VDR or RAR γ (Fig. 5b and c). RXR α and β ablation (Fig. 5d), which releases both heterodimers from their binding sites, abolishes this repression and allows basal promoter-bound transcription factors to stimulate TSLP transcription to a basal activity (see Fig. 3f, lane 3) that is sufficient to trigger the generation of an AD-like phenotype (3). Topical application of either active vitamin D3 or a low-calcemic analog (MC903) (Fig. 5e) generates RXR/VDR-coactivator complexes whose transcriptional activity (see Fig. 3f, lane 2) is efficient enough to not only relieve the repression exerted by RXR/RAR γ corepressor complexes but also to further enhance the basal promoter activity. Interestingly, the RXR/RAR γ coactivator complexes formed upon application of BMS961 are much less efficient (Fig. 5f), because they generate lower TSLP transcript levels (Fig. 1a) than those resulting from the basal promoter activity, as observed in keratinocytes ablated for RXR α and β (see Fig. 3f, lane 3). However, upon cotreatment with BMS961 and a limiting dose of 1 α ,25-(OH) $_2$ D $_3$ (Fig. 5g), liganded RXR/RAR γ and RXR/VDR heterodimers can efficiently synergize to enhance the activity of TSLP basal promoter.

It should be stressed that, even though the present model accounts for all of our present observations, its refinement will require additional genetic (selective ablation of both VDR and

RAR γ in epidermal keratinocytes; mutation of the putative VDRE and RARE in the mouse) and biochemical (e.g., ChIP assays) studies to determine to which elements the RXR/VDR and RXR/RAR heterodimers bind, and whether VDR or RAR γ preferentially heterodimerize with RXR α or RXR β . In any event, the rapid and regulable induction of TSLP in mouse keratinocytes upon topical treatment with low-calcemic vitamin D3 analogs (e.g., MC903) provides a highly convenient AD preclinical model for exploring therapeutic avenues as well as a mouse model allowing characterization of various aspects of AD pathogenesis from its onset to the fully established disease phenotype. In this respect, we have found that epidermal thickening and dermal infiltration are observed in MC903-treated skin of both WT and RAG1 $^{-/-}$ mice lacking mature T and B cells, showing that, even though 1 α ,25-(OH) $_2$ D $_3$ could directly enhance the formation of Th2 cells from naive CD4 $^+$ T cells (18), these cells are actually not required for TSLP-induced development of an AD-like inflammation. Thus, the presence of eosinophils, mast cells, and dermal dendritic cells in MC903-treated RAG1 $^{-/-}$ mice suggests that TSLP could act directly on these and other myeloid-derived cells to initiate an atopic inflammation, whereas the additional accumulation of CD4 $^+$ Th2 cells in MC903-treated WT mice may correspond to a secondary effect of TSLP expression that serves for further progression of the AD-like phenotype. A similar conclusion was recently reached by Yoo *et al.* (8) using TCR $\beta^{-/-}$ mice that lack T cells. As expected, no IgE could be detected in both MC903-treated and untreated RAG1 $^{-/-}$ mice, indicating that IgE are dispensable for development of the AD-like phenotype, in keeping with the observation that, although elevated serum IgE is a frequently associated clinical feature in AD, \approx 20% of AD patients have a normal serum IgE level (4).

Recent reports (5–9), including ours (3), have shown that TSLP represents a master switch of allergic inflammation and established in the mouse a direct link between TSLP expression in keratinocytes and airway epithelial cells and the pathogenesis of atopic dermatitis and asthma, respectively. However, how TSLP expression is triggered in these cells upon allergen exposure remains to be unveiled. Our previous (3) and present reports indicate that RXR heterodimerized with VDR and RAR γ actively suppress TSLP expression, whereas active vitamin D3 and, to a lesser extent, RA can relieve this repression, thus raising the question of whether and how these ligands could be instrumental in triggering TSLP production *in vivo*. In this respect, a possible direct involvement of vitamin D signaling in atopy is supported by the observation that VDR-null mutant mice fail to develop symptoms of experimental asthma (23). Furthermore, vitamin A deficiency is known to diminish Th2-mediated responses, whereas high dietary vitamin A enhances them (24), which may reflect a role of RA-liganded RAR in TSLP induction.

Under homeostatic conditions *in vivo*, epidermal keratinocytes lack RA (11, 25). In keeping with a very low level of TSLP transcripts, others (refs. 14 and 26 and references therein) have shown that there is very little, if any, active vitamin D3 in these cells in which the enzyme 25(OH)D $_3$ -1 α -hydroxylase, required for synthesis of 1 α ,25-(OH) $_2$ D $_3$ from 25(OH)D $_3$, is apparently not expressed. What could then be the origin of active vitamin D3 that induces TSLP expression in atopic dermatitis? Interestingly, it has been recently reported that, upon microbe-derived ligand activation of their Toll-like receptors (TLRs) that mediate the synthesis of antimicrobial peptides involved in the innate immune response, human, but not mouse, macrophages can produce 25(OH)D $_3$ -1 α -hydroxylase and synthesize 1 α ,25-(OH) $_2$ D $_3$ (27, 28). We suggest that similar activation by allergen-derived ligands, of skin macrophage, dendritic cell, or, possibly, keratinocyte TLRs (29–31) may provide 1 α ,25-(OH) $_2$ D $_3$ to keratinocytes in either a paracrine or autocrine manner. Thus, upon exposure of skin to an allergen, TSLP production might be triggered through a TLR-mediated production of active vitamin D3, raising the interesting possibility

that genetic or acquired defects of TLRs' function could be implicated in the pathogenesis of AD. Whether, upon allergen exposure, a TLR-mediated mechanism might also be involved in the production of RA is unknown.

That vitamin D could be instrumental to the pathogenesis of atopic diseases in humans is supported by an association between vitamin D supplementation in infancy and an increased risk of atopy later in life (32, 33). Our present study indicates that this association could be related to an increase of TSLP production in epithelial cells upon exposure to allergens during the perinatal period, which may ultimately result in an increase of allergen-specific Th2 memory cells which could be instrumental to triggering allergic reactions later in life. Interestingly, genetic investigations have also indicated that vitamin D signaling could be implicated in the pathogenesis of atopic diseases, as shown by association of VDR genetic variants with childhood and adult asthma, and atopic response (34, 35). These observations suggest that genetic predisposition to atopic disorders may implicate alteration of other components of vitamin D (and possibly vitamin A) signaling, which will ultimately result in TSLP overproduction. Dysregulation of vitamin D signaling may therefore be a key contributor to both genetic and environmental factors that underlie atopic diseases.

The therapeutic use of vitamins D and A has been considered for AD patients (36–39). Our present data indicate that, on the contrary, administration of these vitamins may exacerbate AD and, very likely, asthma by promoting expression of TSLP in skin and lungs. On the other hand, topical administration of vitamins D and/or A antagonists to AD patients may be beneficial, because it could enhance the repression exerted by RXR/VDR and RXR/RAR γ heterodimers (40) on TSLP expression. It has also been recently suggested that low-calcemic VDR agonists (e.g., MC903) could be used to boost the innate immune response (through enhanced antimicrobial peptide production), for instance, to protect against infections and to accelerate wound healing, notably in the case of chronic ulcerated skin wounds (28, 39, 41, 42). Our results indicate that such therapy may not be beneficial to patients prone to atopy. Finally, our study also provides insight into the

molecular mechanism that could underlie the use of low-calcemic vitamin D analogs in the treatment of psoriasis (13), a Th1 cell-driven skin disease. Interestingly, the most-common side effect of this treatment is a skin irritation (red, dry, and itchy skin) (43) exhibiting similarities with AD lesions. What our data, therefore, suggest is that a Th1 to Th2 skewing of Th cell differentiation triggered by induction of TSLP expression in keratinocytes may contribute to the therapeutic effect of topical MC903 on psoriatic lesions.

Methods

Experimental Animals and Skin Topical Application. VDR^{-/-} (17), RXR α β ^{ep-/-} (tamoxifen-treated K14-Cre-ER^{T2(tg0)}/RXR α ^{L2/L2}/RXR β ^{L2/L2}) (3), and RAG1^{-/-} mice (The Jackson Laboratory) were as described. VDR^{ep-/-} (K14-Cre^(tg0)/VDR^{L2/L2}) mice were obtained by crossing K14-Cre^(tg0) transgenic mice (16) with floxed VDR^{L2/L2} mice (our unpublished data). 1 α ,25-(OH)₂D₃ (Biomol), MC903 (12), and BMS961 (11) were dissolved in ethanol and topically applied on ears or shaved dorsal skin (1 cm²) of either 6- to 8-week-old female CD1 WT mice or mice with indicated genotypes.

Other Methods. Histopathology, IHC, RNA analysis, serum cytokine and Ig determination, hematology assays, and statistic analysis are described in *Supporting Materials and Methods*, which is published as supporting information on the PNAS web site.

We thank the staff of the mouse, histopathology, hematology, and transgenic facilities and the Secretariat of the Institut de Génétique et de Biologie Moléculaire et Cellulaire (IGBMC) and Institut Clinique de la Souris for their kind help; Drs. N. Rochel-Guiberteau (IGBMC) and D. Moras (IGBMC) for vitamin D3 analogs; Bristol Meyer Squibb for BMS961; Dr. S. Chan (IGBMC) for RAG1^{-/-} mice and helpful discussion; and Dr. F. Geissmann for a critical reading of the manuscript. This work was supported by funds from the Centre National de la Recherche Scientifique, the Institut National de la Santé et de la Recherche Médicale, the Collège de France, the Ministère de la Recherche, and European Community Project EUMORPHIA PLRT-CT-2001-00930.

- Laudet, V. & Gronemeyer, H. (2002) *The Nuclear Receptor: Factsbook* (Academic, San Diego).
- Mangelsdorf, D. J., Thummel, C., Beato, M., Herrlich, P., Schutz, G., Umesono, K., Blumberg, B., Kastner, P., Mark, M., Chambon, P., et al. (1995) *Cell* **83**, 835–839.
- Li, M., Messaddeq, N., Teletin, M., Pasquali, J. L., Metzger, D. & Chambon, P. (2005) *Proc. Natl. Acad. Sci. USA* **102**, 14795–14800.
- Leung, D. Y., Boguniewicz, M., Howell, M. D., Nomura, I. & Hamid, Q. A. (2004) *J. Clin. Invest.* **113**, 651–657.
- Soumelis, V., Reche, P. A., Kanzler, H., Yuan, W., Edward, G., Homey, B., Gilliet, M., Ho, S., Antonenko, S., Lauerma, A., et al. (2002) *Nat. Immunol.* **3**, 673–680.
- Liu, Y. J. (2006) *J. Exp. Med.* **203**, 269–273.
- Zhou, B., Comeau, M. R., De Smedt, T., Liggitt, H. D., Dahl, M. E., Lewis, D. B., Gyarmati, D., Aye, T., Campbell, D. J. & Ziegler, S. F. (2005) *Nat. Immunol.* **6**, 1047–1053.
- Yoo, J., Omori, M., Gyarmati, D., Zhou, B., Aye, T., Brewer, A., Comeau, M. R., Campbell, D. J. & Ziegler, S. F. (2005) *J. Exp. Med.* **202**, 541–549.
- Al-Shami, A., Spolski, R., Kelly, J., Keane-Myers, A. & Leonard, W. J. (2005) *J. Exp. Med.* **202**, 829–839.
- Perissi, V. & Rosenfeld, M. G. (2005) *Nat. Rev. Mol. Cell Biol.* **6**, 542–554.
- Chapellier, B., Mark, M., Messaddeq, N., Calleja, C., Warot, X., Brocard, J., Gerard, C., Li, M., Metzger, D., Ghyselinck, N. B., et al. (2002) *EMBO J.* **21**, 3402–3413.
- Carlberg, C. (2003) *J. Cell. Biochem.* **88**, 274–281.
- Kragballe, K. & Iversen, L. (1993) *Dermatol. Clin.* **11**, 137–141.
- Jones, G., Strugnell, S. A. & DeLuca, H. F. (1998) *Physiol. Rev.* **78**, 1193–1231.
- Carlberg, C., Mathiasen, I. S., Saurat, J. H. & Binderup, L. (1994) *J. Steroid Biochem. Mol. Biol.* **51**, 137–142.
- Li, M., Chiba, H., Warot, X., Messaddeq, N., Gerard, C., Chambon, P. & Metzger, D. (2001) *Development (Cambridge, U.K.)* **128**, 675–688.
- Yoshizawa, T., Handa, Y., Uematsu, Y., Takeda, S., Sekine, K., Yoshihara, Y., Kawakami, T., Arioka, K., Sato, H., Uchiyama, Y., et al. (1997) *Nat. Genet.* **16**, 391–396.
- Boonstra, A., Barrat, F. J., Crain, C., Heath, V. L., Savelkoul, H. F. & O'Garra, A. (2001) *J. Immunol.* **167**, 4974–4980.
- Mombaerts, P., Iacomini, J., Johnson, R. S., Herrup, K., Tonegawa, S. & Papaioannou, V. E. (1992) *Cell* **68**, 869–877.
- Wang, T. T., Tavera-Mendoza, L. E., Laperriere, D., Libby, E., MacLeod, N. B., Nagai, Y., Bourdeau, V., Konstorum, A., Lallemand, B., Zhang, R., et al. (2005) *Mol. Endocrinol.* **19**, 2685–2695.
- Chambon, P. (2005) *Mol. Endocrinol.* **19**, 1418–1428.
- Leid, M., Kastner, P. & Chambon, P. (1992) *Trends Biochem. Sci.* **17**, 427–433.
- Wittke, A., Weaver, V., Mahon, B. D., August, A. & Cantorna, M. T. (2004) *J. Immunol.* **173**, 3432–3436.
- Stephensen, C. B. (2001) *Annu. Rev. Nutr.* **21**, 167–192.
- Calleja, C., Messaddeq, N., Chapellier, B., Yang, H., Krezel, W., Li, M., Metzger, D., Mascrez, B., Ohta, K., Kagechika, H., et al. (2006) *Genes Dev.* **20**, 1525–1538.
- Vanhooke, J. L., Prah, J. M., Kimmel-Jehan, C., Mendelsohn, M., Danielson, E. W., Healy, K. D. & DeLuca, H. F. (2006) *Proc. Natl. Acad. Sci. USA* **103**, 75–80.
- Kupper, T. S. & Fuhlbrigge, R. C. (2004) *Nat. Rev. Immunol.* **4**, 211–222.
- Liu, P. T., Stenger, S., Li, H., Wenzel, L., Tan, B. H., Krutzik, S. R., Ochoa, M. T., Schaub, J., Wu, K., Meinken, C., et al. (2006) *Science* **311**, 1770–1773.
- Fritsche, J., Mondal, K., Ehrnsperger, A., Andreesen, R. & Kreutz, M. (2003) *Blood* **102**, 3314–3316.
- Takeda, K., Kaisho, T. & Akira, S. (2003) *Annu. Rev. Immunol.* **21**, 335–376.
- Chu, A. C. & Morris, J. F. (2005) in *Skin Immune System*, ed. Bos, J. D. (CRC, Boca Raton, FL), pp. 77–99.
- Wjst, M. & Dold, S. (1999) *Allergy* **54**, 757–759.
- Hyponen, E., Sovio, U., Wjst, M., Patel, S., Pekkanen, J., Hartikainen, A. L. & Jarvelin, M. R. (2004) *Ann. N.Y. Acad. Sci.* **1037**, 84–95.
- Poon, A. H., Laprise, C., Lemire, M., Montpetit, A., Sinnett, D., Schurr, E. & Hudson, T. J. (2004) *Am. J. Respir. Crit. Care Med.* **170**, 967–973.
- Raby, B. A., Lazarus, R., Silverman, E. K., Lake, S., Lange, C., Wjst, M. & Weiss, S. T. (2004) *Am. J. Respir. Crit. Care Med.* **170**, 1057–1065.
- Worm, M. (2002) *Curr. Opin. Investig. Drugs* **3**, 1596–1603.
- Lehmann, B., Querings, K. & Reichrath, J. (2004) *Exp. Dermatol.* **13**, Suppl 4, 11–15.
- Zasloff, M. (2005) *J. Invest. Dermatol.* **125**, xvi–xvii.
- Zasloff, M. (2006) *Nat. Med.* **12**, 388–390.
- Germain, P., Iyer, J., Zechel, C. & Gronemeyer, H. (2002) *Nature* **415**, 187–192.
- Gombart, A. F., Borregaard, N. & Koeffler, H. P. (2005) *Faseb J.* **19**, 1067–1077.
- Wang, T. T., Nestel, F. P., Bourdeau, V., Nagai, Y., Wang, Q., Liao, J., Tavera-Mendoza, L., Lin, R., Hanrahan, J. H., Mader, S., et al. (2004) *J. Immunol.* **173**, 2909–2912.
- Gottlieb, A. B. (2005) *J. Am. Acad. Dermatol.* **53**, S3–S16.

Turning Off Estrogen Receptor β -Mediated Transcription Requires Estrogen-Dependent Receptor Proteolysis[∇]

Yukiyo Tateishi,^{1†} Raku Sonoo,^{2†} Yu-ichi Sekiya,¹ Nanae Sunahara,¹ Miwako Kawano,¹ Mitsutoshi Wayama,¹ Ryuichi Hirota,² Yoh-ichi Kawabe,¹ Akiko Murayama,¹ Shigeaki Kato,³ Keiji Kimura,¹ and Junn Yanagisawa^{1,2*}

Graduate School of Life and Environmental Sciences, University of Tsukuba, Tsukuba Science City, Ibaraki 305-8572, Japan¹; Anlks Incorporated, Tsukuba Industrial Liaison and Cooperative Research Center, University of Tsukuba, Tsukuba Science City, Ibaraki 305-8577, Japan²; and Institute of Molecular and Cellular Biosciences, University of Tokyo, Bunkyo-ku, Tokyo 113-0032, Japan³

Received 25 April 2006/Returned for modification 12 June 2006/Accepted 17 August 2006

Recent studies have shed light on the ligand-dependent transactivation mechanisms of nuclear receptors (NRs). When the ligand dose is reduced, the transcriptional activity of NRs should be downregulated. Here we show that a ubiquitin-proteasome pathway plays a key role in turning off transcription mediated by estrogen receptor β (ER β). ER β shows estrogen-dependent proteolysis, and its degradation is regulated by two regions in the receptor. The N-terminal 37-amino acid-region is necessary for the recruitment of the ubiquitin ligase, i.e., the carboxyl terminus of HSC70-interacting protein (CHIP), to degrade ER β . In contrast, the C-terminal F domain protects ligand-unbound ER β from proteolysis to abrogate proteasome association. Suppression of CHIP by interfering RNA inhibited this switching off of receptor-mediated transcription when the ligand dose was reduced. Our results suggest that after ligand withdrawal, the active form of the NR is selectively eliminated via ligand-dependent proteolysis to downregulate receptor-mediated transcription.

Estrogen is a growth factor that stimulates cell growth and differentiation in diverse tissues. Dramatic changes in the levels of estrogen in the blood occur during the normal human menstrual cycle. During the first 7 to 10 days, the level of estrogen is low. In the middle of the cycle (days 11 to 15), it rises and then falls abruptly. The effects of estrogen are mediated through the estrogen receptors (ERs), ER α and ER β , which function as ligand-induced transcription factors and belong to the nuclear receptor (NR) superfamily (2, 5, 12, 20, 31, 33, 41, 49). When the estrogen level is high, estrogen binds to ERs to activate the transcription of target genes. This induces the ligand-binding domain (LBD) to undergo a characteristic conformational change, whereupon the receptor dimerizes, binds to DNA, and subsequently stimulates gene expression (10). ER α is stimulated by two distinct activation regions, activation function 1 (AF-1) and AF-2, which are located in the LBD and exert ligand-dependent transcriptional activity. Crystal structure analysis of ERs and other NRs has revealed the presence of 12 conserved helices in their LBDs (46). The LBD forms a structure described as a sandwich of 12 α -helices (helices 1 to 12) with a central hydrophobic ligand-binding pocket. Helix 12, the most C-terminal of these helices, has been identified as the critical core (AD core) of the AF-2 function of the receptor and plays an important role in coactivator binding to the ligand-bound receptor (6, 19, 24, 25, 33, 35, 39, 43, 45, 55, 56).

When the level of estrogen is decreased, receptor-mediated transcription should be downregulated. Because the response to estrogen is tightly controlled, the downregulation of ER-mediated transcription should also be tightly regulated. Although such regulation of the NRs has generated intense interest, the molecular mechanisms regulating these processes are not understood (38). To switch off transcription, there are at least two possible mechanisms. The first involves the dissociation of ligands from the hormone-binding pocket of the receptor. However, the dissociation rate of the ligand from its receptor is very low, because the receptor locks the hormone within its activation pocket and covers it with coactivators (16). Another possible mechanism is the rapid degradation of active receptors. Several nuclear receptors, such as the ER and those for progesterone, glucocorticoid, thyroid hormone receptor, retinoid X, and retinoic acid, are ubiquitinated and degraded in the course of their nuclear activities (8, 11, 13, 26, 29, 32, 36, 47, 51, 57). These degradation steps might be involved in turning off NR-mediated transcription.

Evidence now suggests that proteasome-dependent degradation of receptors is necessary for the activation of these receptors (38). Moreover, this requires NR-mediated transcriptional activity, implying that the degradation and the transactivation of NRs are mutually independent processes. In the ubiquitin-proteasome pathway, proteins destined for degradation are conjugated by polyubiquitin chains, in which one ubiquitin molecule is conjugated by another through one of its seven lysine residues, typically K48. These polyubiquitin chains are then recognized by the regulatory complex of the 26S proteasome.

Here we show that there is a ubiquitin-proteasome pathway for ER β that is not coupled to transactivation. To investigate this, we purified the ubiquitin ligase complex for ER β and

* Corresponding author. Mailing address: Graduate School of Life and Environmental Sciences, University of Tsukuba, Tsukuba Science City, Ibaraki 305-8572, Japan. Phone: 81-29-853-6632. Fax: 81-29-853-4605. E-mail: junny@agbi.tsukuba.ac.jp.

† These authors contributed equally to this work.

∇ Published ahead of print on 28 August 2006.

identified a protein complex containing the carboxyl terminus of heat shock cognate 70 (HSC70)-interacting protein (CHIP) (1). CHIP binds directly to the N-terminal 37-amino-acid region of ER β and ubiquitinates it to induce ER β degradation. In contrast, the C-terminal F domain inhibits the binding of proteasome to the receptor and protects it from proteolysis in the absence of estrogen. Suppression of CHIP by interfering RNA (RNAi) inhibited the switching off of receptor-mediated transcription that occurs when the ligand dose is reduced. Our results suggest that ligand-dependent degradation selectively and rapidly eliminates the active form of a nuclear receptor to downregulate receptor-mediated transcription after ligand withdrawal.

MATERIALS AND METHODS

Expression vectors. The ER α/β and CHIP expression plasmids and their deletion mutants have been described previously (48). ERE-TATA-Luc and ERE-TATA-LucCP were constructed by inserting three consensus estrogen response elements into a luciferase reporter plasmid encoding a TATA box, pGL3-Basic or pHRG(R2.2)-Basic. pGL3-Basic, pHRG(R2.2)-Basic, and pGL3-Control vectors were purchased from Promega (Madison, WI).

Antibodies. Anti-FLAG-M2 mouse monoclonal antibody (Sigma, St. Louis, MO), anti-hemagglutinin (HA) mouse monoclonal antibody (Roche), anti-human ER α antibody (Chemicon, Temecula, CA), anti-human ER β antibody (PPMX), and anti-glyceraldehyde-3-phosphate-dehydrogenase mouse monoclonal antibody (American Research Products, Inc.) were used at appropriate dilutions, according to the manufacturers' instructions. A rabbit polyclonal antibody directed against CHIP was provided by T. Chiba (Tokyo Metropolitan Institute of Medical Science).

Cell culture and transfection. MDA-MB231 breast cancer cells and human embryonic kidney 293 cells were routinely maintained in Dulbecco's modified Eagle's medium (DMEM) supplemented with 10% fetal bovine serum (FBS). Twenty-four hours before transfection, the medium was changed to phenol red-free DMEM containing 4% charcoal-stripped FBS. Transfection was performed using PerFectin transfection reagent (Gene Therapy Systems) or TransFast transfection reagent (Promega) according to the manufacturers' protocols. The cells were treated with or without MG132 (10^{-6} M) and estrogen (10^{-8} M). Twenty-four hours after the addition of estrogen, the cells were harvested and analyzed by Western blotting using the appropriate antibodies.

Coimmunoprecipitation and Western blotting. The 293 cells were transfected with the appropriate plasmids and lysed in TNE buffer (10 mM Tris-HCl [pH 7.8], 0.5% Nonidet P-40 [NP-40], 0.15 M NaCl, 1 mM EDTA, 1 μ M phenylmethylsulfonyl fluoride [PMSF], 1 μ g/ml aprotinin). Extracted proteins were immunoprecipitated with antibody-coated protein A/G-Sepharose (Amersham) or anti-FLAG M2 agarose (Sigma). The bound proteins were separated by sodium dodecyl sulfate-polyacrylamide gel electrophoresis (SDS-PAGE), transferred onto polyvinylidene difluoride membranes (Millipore), and detected with the appropriate antibodies and secondary antibodies conjugated with horseradish peroxidase. Specific proteins were detected using an enhanced chemiluminescence Western blot detection system (Amersham).

Luciferase assay. For luciferase assays, ERE-TATA-Luc plasmids were cotransfected with expression vector encoding ER β or its mutants. As a reference plasmid with which to normalize transfection efficiency, the pRSV β GAL vector or the pRL-CMV vector was cotransfected in all experiments. Twenty-four hours after transfection, the culture medium was replaced with fresh medium containing 0.2% FBS, either estrogen (10^{-8} M) or ethanol vehicle was added, and the cells were incubated for an additional 24 h. Cell extracts were prepared, and luciferase assays were performed following the manufacturer's protocol (Promega). β -Galactosidase activity was measured to control for the efficiency of each transfection. Individual transfections, each consisting of triplicate wells, were repeated at least three times.

Protein purification. Glutathione S-transferase (GST) protein or an immobilized 37-amino-acid region that we designated the "domain required for degradation" (DRD) fused to GST (GST-DRD) was preincubated for 1 h at 4°C in GST-binding buffer (20 mM Tris-HCl [pH 7.9], 180 mM KCl, 0.2 mM EDTA, 0.5 mM PMSF, and 1 mM dithiothreitol) containing bovine serum albumin (BSA; 1 mg/ml). Bead-immobilized proteins were then incubated at 4°C for 6 to 10 h with 293 cell extracts. After the beads had been washed three times with GST buffer (GST-binding buffer with 0.1% NP-40), they were washed again with GST buffer

containing 0.2% *N*-lauroyl sarcosine. Proteins bound to the DRD were eluted with 15 mM reduced glutathione in elution buffer (50 mM Tris-HCl [pH 8.3], 150 mM KCl, 0.5 mM EDTA, 0.5 mM PMSF, 5 mM NaF, 0.08% NP-40, 0.5 mg/ml BSA, and 10% glycerol). Recombinant CHIP was expressed in *Escherichia coli* and purified using Ni-agarose.

Immunofluorescence. The 293 cells were grown on poly-L-lysine-coated 12-well culture dishes and transfected with plasmids. Twenty-four hours after transfection, the cells were fixed with 4% paraformaldehyde in phosphate-buffered saline (PBS) for 10 min and permeabilized with Triton buffer (50 mM Tris-HCl [pH 7.5], 0.5% Triton X-100, 150 mM NaCl, 2 mM EDTA) for 15 min. The cells in each well were blocked with PBS containing 1% BSA and 0.5% goat serum for 3 h at 37°C. The cells were incubated with the appropriate antibody in PBS containing 1% BSA for 2 h at 37°C. After the cells had been washed with PBS, they were incubated with Alexa-Fluor-488-conjugated goat anti-rat immunoglobulin G or Alexa-Fluor-594-conjugated goat anti-mouse immunoglobulin G (Molecular Probes) for 1 h at 37°C and washed with PBS. The samples were mounted with Vectashield mounting medium (Vector Laboratories) and analyzed using a Keyence Biozero BZ-8000.

Pulse-chasing. The 293 cells were transfected with ER β , and 48 h after transfection the cells were labeled for 30 min at 37°C with [³⁵S]methionine (50 μ Ci/ml) in methionine-free DMEM. The cells were then washed twice and incubated in DMEM containing 0.2% FBS for the indicated periods (chase). At each time point, cell lysates were immunoprecipitated with anti-ER β antibody. The immunoprecipitates were resolved by SDS-PAGE and visualized by autoradiography. A phosphorimager was used to quantify the metabolically labeled ER β present at each time point.

RNAi. The 293gp cells were transfected with pSINsi-hU6 vector (Takara) containing the target sequence of CHIP or LacZ (control) and with vesicular stomatitis virus-encoded envelope protein G to generate the small interfering RNA (siRNA) retroviral supernatant. MDA-MB-231 cells were transfected with retroviral supernatant in the presence of Polybrene (8 μ g/ml). Twenty-four hours after transfection, the viral supernatant was replaced with fresh DMEM containing 10% FBS. The transfected cells were selected with G418 (1 mg/ml). The target sequences were 5'-GCACGACAAGTACATGGCGGA-3' for CHIP and 5'-GCTACACAAATCAGCGATT-3' for LacZ.

RESULTS

An N-terminal 37-amino-acid region is essential for ER β degradation. The level of ER β protein was reduced by the addition of estrogen to the MDA-MB-231 breast cancer cell line. This degradation was inhibited by the proteasome inhibitors MG132 (Fig. 1A) and lactacystin (data not shown). In a ubiquitination assay, ER β was ubiquitinated in both the presence and the absence of estrogen (Fig. 1B). Thus, ER β is degraded via ubiquitin-proteasome pathways. Preliminary biochemical study showed that a single K48-linked polyubiquitin chain is sufficient to target a substrate to the 26S proteasome. Therefore, we investigated the ubiquitin lineage of the chains using a ubiquitin mutant lacking specific lysines, Ub(K48R). HA-tagged ubiquitin (HA-Ub) or Ub(K48R) was transfected into 293 cells, and the level of ER β protein and the ubiquitination status were determined by Western blotting using an anti-FLAG-M2 or an anti-HA antibody. Expression of Ub(K48R) reduced the degradation (Fig. 1C) and the ubiquitination status (Fig. 1D) of ER β , suggesting that the polyubiquitin chains of ER β are linked via K48. These results indicate that whereas ER β is polyubiquitinated via K48 in ubiquitin in both the presence and the absence of estrogen, the proteolysis is estrogen dependent. Our observations imply that ubiquitination in itself is not the only way to regulate ER β .

To investigate the molecular mechanism by which ER β is degraded, DNA sequences encoding truncated forms of ER α or ER β were transfected into 293 cells, and the protein levels were examined by Western blot analysis. ER α (Δ 181), which does not contain the A/B domain, still underwent

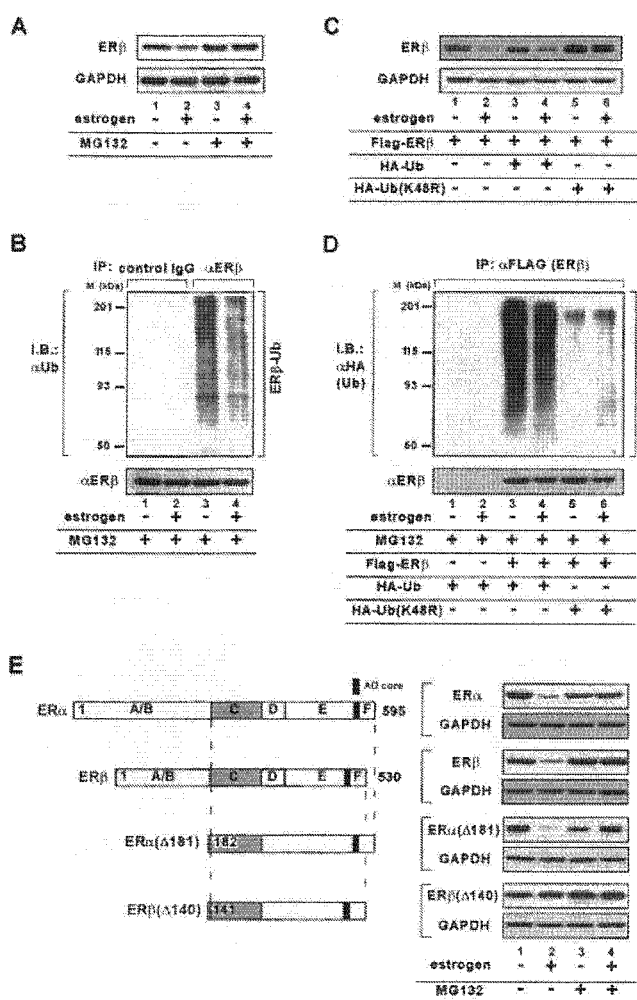


FIG. 1. ERβ is degraded through ubiquitin-proteasome pathways. (A) ERβ is degraded in an estrogen-dependent manner. ERβ-transfected MDA-MB-231 cells were cultured in the presence or the absence of estrogen (10^{-8} M) and the proteasome inhibitor MG132 (10^{-6} M). ERβ level was analyzed by use of Western blots probed with the indicated antibody. (B) ERβ is degraded via ubiquitin-proteasome pathways. ERβ-transfected MDA-MB-231 cells were cultured in the presence or the absence of estrogen (10^{-8} M) and MG132 (10^{-6} M). ERβ was immunoprecipitated (IP) using anti-ERβ antibody. Upper panel: the ubiquitination status of ERβ was analyzed by Western blotting (IB) and probed with an anti-ubiquitin antibody. Lower panel: immunoprecipitated ERβ was detected by Western blotting and probed with an anti-ERβ antibody. IgG, immunoglobulin G; M, molecular mass. (C) The estrogen-dependent degradation of ERβ is inhibited by mutated ubiquitin Ub(K48R). FLAG-tagged ERβ and DNA encoding HA-Ub (1,000 ng) or HA-Ub(K48R) (1,000 ng) were transfected into 293 cells in the presence or the absence of estrogen (10^{-8} M). ERβ was detected by use of Western blots probed with anti-FLAG-M2 antibody. (D) The polyubiquitin chain of ERβ is linked via K48. FLAG-tagged ERβ and DNA encoding HA-Ub (1,000 ng) or HA-Ub(K48R) (1,000 ng) were transfected into 293 cells in the presence or the absence of estrogen (10^{-8} M) and MG132 (10^{-6} M). FLAG-tagged ERβ was immunoprecipitated with anti-FLAG-M2 antibody. Upper panel: the ubiquitination status of ERβ was analyzed by use of Western blots probed with anti-HA antibody. Lower panel: immunoprecipitated ERβ was detected by use of Western blots probed with anti-FLAG antibody. (E) The A/B domain is necessary for the estrogen-dependent degradation of ERβ. DNA (500 ng) encoding the indicated FLAG-tagged ER deletion mutants was transfected into 293 cells. These cells were cultured in the presence or the absence of estrogen (10^{-8} M) and MG132 (10^{-6} M). To evaluate the protein levels of the ER mutants, Western blot analysis was performed using anti-FLAG-M2 antibody.

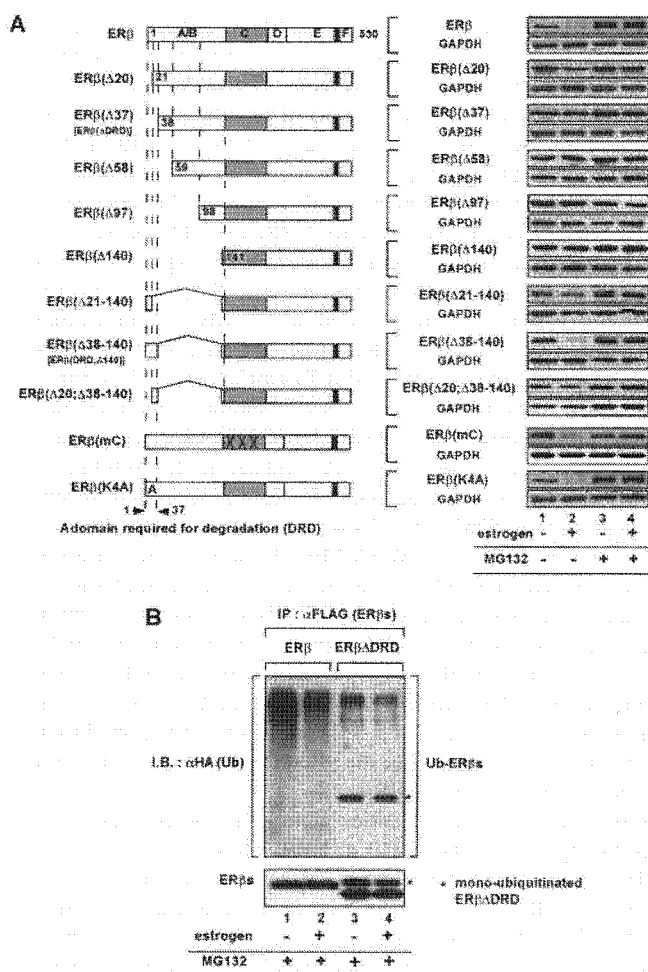


FIG. 2. DRD-mediated degradation is involved in the downregulation of ERβ-mediated transcription. (A) The N-terminal 37-amino-acid region is essential for estrogen-mediated ERβ degradation. DNA sequences (500 ng) encoding the indicated FLAG-tagged ERβ deletion mutants were transfected into 293 cells. These cells were cultured in the presence or the absence of estrogen (10^{-8} M) and MG132 (10^{-6} M). To evaluate the protein levels of the ERβ mutants, Western blot analysis was performed using an anti-FLAG-M2 antibody. (B) DRD-regulated ubiquitination of ERβ. DNA (500 ng) encoding the indicated FLAG-tagged ERβ mutants and DNA (1,000 ng) encoding HA-tagged ubiquitin were transfected into 293 cells in the presence or the absence of estrogen (10^{-8} M). Upper panel: FLAG-tagged ERβ mutants were immunoprecipitated (IP) with anti-FLAG-M2 antibody. The ubiquitination status of ERβ was analyzed by use of Western blots probed with anti-HA antibody. Lower panel: immunoprecipitated ERβ mutants were detected by use of Western blots probed with an anti-FLAG-M2 antibody. I.B., Western blotting.

ligand-dependent degradation (Fig. 1E). In contrast, truncation of the A/B domain of ERβ, forming ERβ(Δ140), produced no ligand-dependent degradation, suggesting that the A/B domain of ERβ is necessary for its ligand-dependent degradation (Fig. 1E).

We then investigated the region responsible for the degradation of ERβ. The levels of truncated ERβ protein in the presence and the absence of estrogen were examined by Western blotting. As shown in Fig. 2A, ERβ(Δ20), in which the 20 N-terminal amino acids are deleted, was elevated in the pres-

ence of estrogen compared with wild-type ERβ. ERβ(Δ37) exhibited almost no degradation, indicating that the N-terminal 37 amino acids are essential for the ligand-dependent degradation of ERβ (Fig. 2A). To assess whether this region is sufficient for the ligand-dependent degradation of ERβ, it was fused to ERβ(Δ140), which does not contain the A/B domain and shows little ligand-dependent degradation. In contrast to that of ERβ(Δ140), the level of ERβ(Δ38-140) protein, in which the 37-amino-acid region is fused to ERβ(Δ140), was reduced in an estrogen-dependent manner (Fig. 2A). This reduction was abrogated by the addition of MG132, indicating that ERβ(Δ38-140) is degraded by proteasomal pathways. Interestingly, the degradation of ERβ(mC), which has three amino acid substitutions in the DNA-binding domain (C domain) and has almost no ability to bind DNA (30), was similar to that of wild-type ERβ (Fig. 2A), indicating that binding to the DNA element is not necessary for ligand-dependent receptor degradation. Similar results were obtained when other cell lines, such as MCF-7 or MDA-MB-231, were used (data not shown). From these observations, we concluded that the N-terminal 37-amino-acid region of ERβ is involved in its ligand-dependent degradation and designated this region the DRD. We next determined the ubiquitination status of the truncated forms of ERβ. The DRD deletion accumulated a monoubiquitinated form and showed a reduced level of the polyubiquitinated form (Fig. 2B), suggesting that the DRD is required for the polyubiquitination of ERβ.

Purification and identification of an E3 ubiquitin ligase that specifically binds to the DRD of ERβ. To investigate why the DRD induces ubiquitination, we examined two possibilities. First, the DRD may contain a lysine residue that is ubiquitinated by a ubiquitin ligase specific for ERβ. Second, there may be a ubiquitin ligase that specifically recognizes and binds to the DRD to ubiquitinate ERβ.

To test the first possibility, we introduced an amino acid substitution at the lysine residue in the DRD. ERβ(K4A), in which the lysine residue in the DRD is replaced by alanine, showed ligand-dependent degradation similar to that of the wild type (Fig. 2A), implying that the lysine residue in the DRD is not a target for ubiquitination. Therefore, we investigated the other possibility.

We generated a GST-fused 37-amino-acid region (GST-DRD) with which to purify proteins that specifically bind to the DRD. Whole-cell extracts prepared from 293 cells were incubated with either GST-DRD or GST. The bound proteins were precipitated with glutathione beads and separated using SDS-PAGE (Fig. 3A). Mass fingerprinting methods revealed that the proteins that specifically bound to the DRD were the carboxyl terminus of CHIP, HSP70, and HSP90 (Fig. 3A).

CHIP has E3 ubiquitin ligase activity mediated by its carboxyl-terminal U-box domain and has the ability to bind to chaperones HSP/HSC70 via its tetratricopeptide repeat (TPR) domain (7, 48). A pull-down assay showed that recombinant CHIP bound to the GST-DRD (Fig. 3B). A coimmunoprecipitation assay demonstrated specific binding of CHIP and HSP70 to ERβ in both the absence and the presence of estrogen (Fig. 3C). ERβΔDRD showed no ability to bind CHIP (Fig. 3D). Therefore, we tested whether CHIP enhances ERβ ubiquitination. When ERβ was coexpressed with CHIP, smeary bands of ubiquitin-conjugated ERβ products were observed

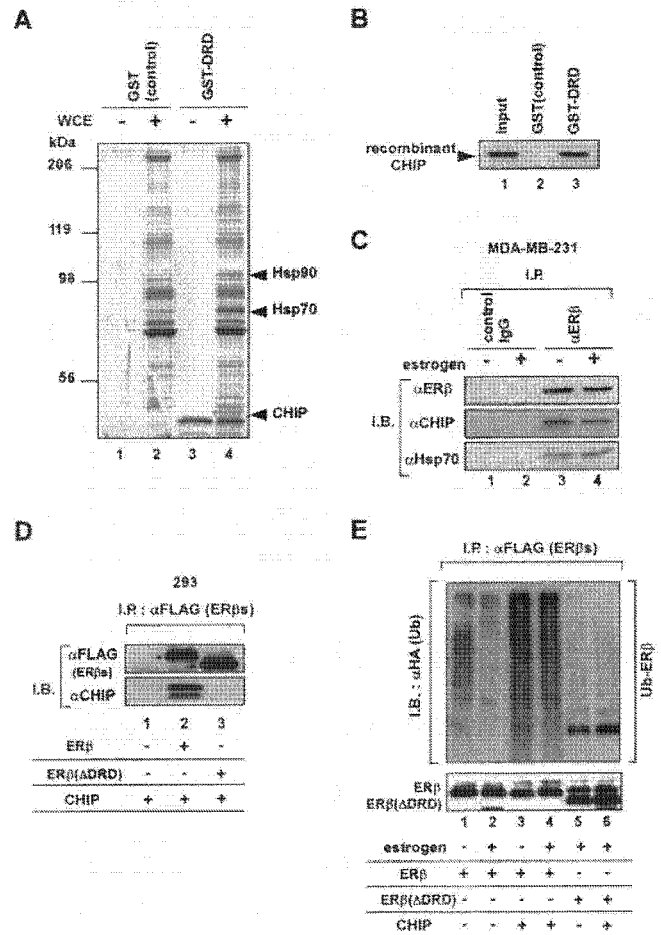


FIG. 3. The DRD associates with a protein complex containing the carboxyl terminus of HSC70-interacting protein (CHIP) and HSC/HSP70. (A) Purification and identification of DRD-interacting proteins. Whole-cell extracts (WCE) prepared from 293 cells were incubated with GST-DRD or with GST as the control. Bound proteins were precipitated with GST-conjugated beads, eluted with glutathione, and subjected to SDS-PAGE followed by silver staining. The fractions eluted from GST and GST-DRD are shown. Proteins eluted from the DRD peptide were examined by mass spectrometry. (B) CHIP binds the DRD. Recombinant CHIP was incubated with GST-DRD or GST. The bound proteins were precipitated with glutathione beads. CHIP bound to GST-DRD was separated by SDS-PAGE. (C) Interaction between ERβ and CHIP in vivo. ERβ-transfected MDA-MB-231 cells were lysed and immunoprecipitated (I.P.) with anti-ERβ antibody in the presence or the absence of estrogen (10^{-8} M). The precipitates were Western blotted (I.B.) and probed with antibodies directed against CHIP and HSP70. IgG, immunoglobulin G. (D) DRD is necessary for the interaction between ERβ and CHIP. ERβ or ERβΔDRD was transfected into 293 cells. These cells were lysed and immunoprecipitated with anti-FLAG-M2 antibody. The precipitates were Western blotted and probed with antibodies directed against CHIP and HSP70. (E) CHIP induces the ubiquitination of ERβ. DNA (500 ng) encoding FLAG-tagged ERβ and DNA (1,000 ng) encoding HA-tagged ubiquitin were transfected into 293 cells with or without DNA (50 ng) encoding CHIP in the presence or the absence of estrogen (10^{-8} M). FLAG-tagged ERβ or ERβ(ΔDRD) was immunoprecipitated using anti-FLAG-M2 antibody. The ubiquitination status of ERβ was analyzed by use of Western blots probed with anti-HA antibody.

(Fig. 3E). In contrast, CHIP expression had no effect on the ubiquitination status of ER β (Δ DRD). Thus, CHIP appears to mediate the ubiquitination of ER β .

CHIP participates in the degradation of ER β . ER β is known to localize predominantly in the nucleus. Although a large proportion of the CHIP protein was localized in the cytoplasm, a small amount was observed in the nucleus by immunostaining (Fig. 4A) and Western blot analysis (Fig. 4B, left panel). To test whether CHIP-mediated ubiquitination induces the degradation of ER β , DNA encoding ER β was transfected into 293 cells with or without DNA encoding CHIP. Western blot analysis revealed that the steady-state level of ER β decreased in both the nucleus and the cytoplasm when CHIP was produced (Fig. 4B, left panel). ER β in MDA-MB-231 cells also decreased with the production of CHIP (Fig. 4B, right panel). We further determined CHIP's function by producing MDA-MB-231 cells in which endogenous CHIP expression was suppressed by the introduction of a siRNA complementary to sequences present in the CHIP mRNA. The introduction of the siRNA vector into MDA-MB-231 cells suppressed the expression of CHIP mRNA (data not shown) and protein (Fig. 4C, left panel) and the accumulation of ER β protein (Fig. 4C, right panel). In contrast, a control vector failed to alter the CHIP or ER β protein levels (Fig. 4C, right panel). Thus, CHIP appears to be involved in estrogen-dependent ER β degradation. To confirm this, pulse-chase experiments were performed. In the presence of estrogen, the half-life of ER β exceeded 8 h, but it had a half-life of about 4 h when CHIP was expressed (Fig. 4D).

To confirm that the DRD is necessary for CHIP-dependent ER β degradation, DNA sequences encoding truncated forms of ER β were transfected into 293 cells with or without DNA encoding CHIP. CHIP expression enhanced the degradation of ER β , ER β (mC), ER β (DRD; Δ 140), and ER β (AF-1), all of which contain the DRD, but did not enhance the degradation of ER β (Δ DRD) or ER β (Δ 140), neither of which contains the DRD (Fig. 5A). To test the specificity of this effect, we created constructs in which the TPR and U-box domains of CHIP were deleted (Δ TPR and Δ U-box, respectively). CHIP binds to HSP/HSC70 via its TPR motif and displays E3 ubiquitin ligase activity mediated by its U-box domain. Although the expression of these truncated proteins was similar to that of full-length CHIP (data not shown), deletion of either of these domains abolished the effects of CHIP on ER β (Fig. 5B). Such a requirement for a TPR motif indicates that CHIP may have to interact with HSP/HSC70 to promote ER β degradation. The functional requirement for the U-box confirms that CHIP regulates ER β ubiquitination.

In a previous report, we showed that CHIP binds ER α in the absence of estrogen (48). Since ER α and ER β heterodimerize readily in the presence of each other, we examined the effect of coinfecting ER α on CHIP-dependent degradation of ER β . As shown in Fig. 5C, the degradation of ER β was not affected by coexpression of ER α .

The F domain regulates ER β degradation negatively. Our results showed that whereas CHIP binds and ubiquitinates ER β in both the presence and the absence of estrogen, the degradation of ER β is estrogen dependent. To investigate this discrepancy, DNA sequences encoding truncated forms of ERs were transfected into 293 cells and the protein levels were

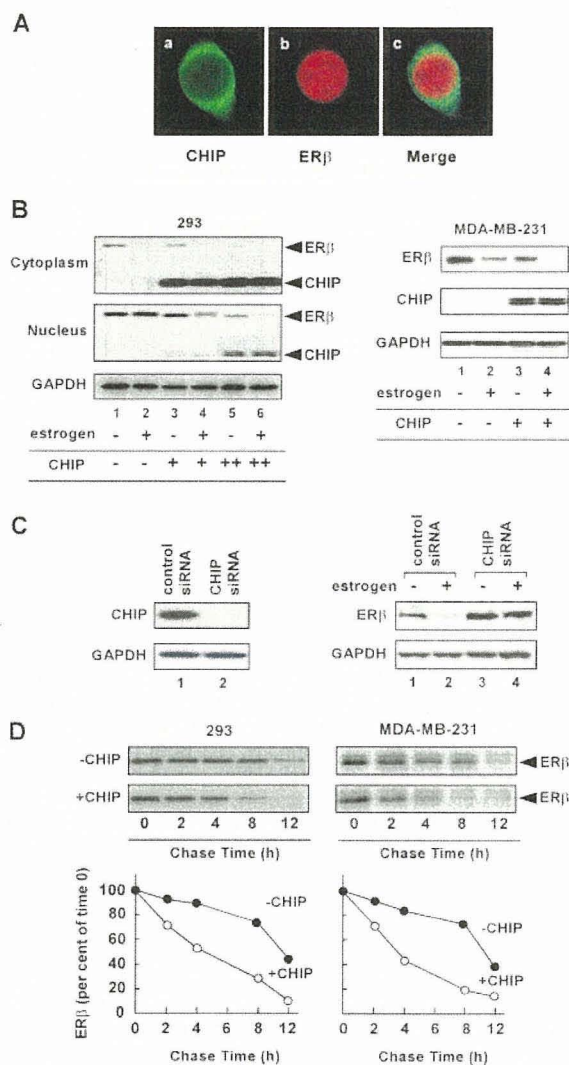


FIG. 4. CHIP enhances the degradation of ER β . (A) CHIP protein was observed in both the cytoplasm and the nucleus. The 293 cells were transiently transfected with plasmids encoding HA-tagged CHIP and FLAG-tagged ER β . Mounted cells were examined by immunofluorescence microscopy as described in Materials and Methods. (a) The distribution of CHIP in the cell is shown. (b) The distribution of ER β is shown. (c) Merged images of panels a and b. (B) CHIP expression reduced the steady-state level of ER β . DNA (50 ng) encoding HA-tagged CHIP was cotransfected into 293 or MDA-MB-231 cells with DNA (500 ng) encoding FLAG-tagged ER β in the absence or the presence of estrogen (10^{-8} M). The level of ER β protein was examined by use of Western blots probed with anti-FLAG (293) or anti-ER β (MDA-MB-231) antibody. (C) ER β accumulated after the siRNA-mediated suppression of endogenous CHIP. Plasmids encoding a siRNA specific for CHIP or the control vector were introduced into MDA-MB-231 cells. These cells were selected with G418. Levels of CHIP and ER β proteins were assessed by immunoblotting the whole-cell lysates with specific antibodies, as indicated. (D) CHIP facilitates the degradation of ER β . 293 or MDA-MB-231 cells were transfected with DNA (50 ng) encoding CHIP or with DNA (500 ng) encoding FLAG-tagged ER β in the presence of estrogen (10^{-8} M). Cells were pulse-labeled with [35 S]methionine and then chased for the indicated times in medium containing unlabeled methionine. 35 S-labeled ER β in the immunoprecipitate was quantified by phosphorimaging, and the levels in control cells (closed circles) and CHIP-expressing cells (open circles) were plotted relative to the amount present at time zero.

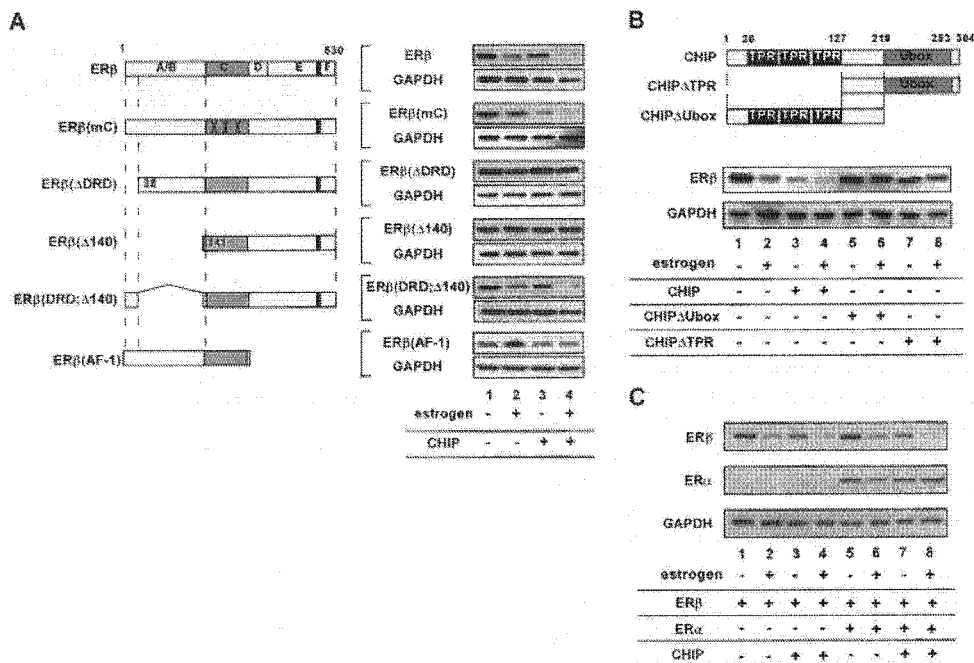


FIG. 5. CHIP regulates DRD-mediated ubiquitination and degradation. (A) The DRD is necessary for CHIP-dependent ER β degradation. DNA (500 ng) encoding the indicated FLAG-tagged ER β mutants was transfected into 293 cells, with or without DNA encoding CHIP. These cells were cultured in the presence or the absence of estrogen (10^{-8} M). To evaluate the levels of ER β mutant proteins, Western blot analysis was performed using anti-FLAG-M2 antibody. (B) Both the TPR and U-box domain of CHIP are necessary for ER β degradation. DNA (50 ng) encoding CHIP, CHIP Δ TPR, or CHIP Δ Ubox was transfected into 293 cells with or without DNA (500 ng) encoding FLAG-tagged ER β . Levels of ER β protein were examined by use of Western blots probed with anti-FLAG-M2 antibody. (C) The CHIP-dependent ER β degradation is not affected by ER α . DNA (500 ng) encoding FLAG-tagged ER β was transfected into 293 cells with or without DNA (500 ng) encoding FLAG-tagged ER α and DNA (50 ng) encoding CHIP. Levels of ER β and ER α protein were examined by use of Western blots probed with anti-FLAG-M2 antibody.

examined. The AD core domain is necessary for estrogen-dependent degradation of ER α (29, 48). Consistent with this observation, ER α (Δ AD) was stabilized by ligand binding and thus accumulated in response to estrogen (Fig. 6A). Interestingly, the deletion of the AD core of ER β resulted in a dramatic reduction in ER β in the absence of estrogen (Fig. 6A). This observation raises the possibility that the C-terminal region of ER β is necessary for the stabilization of ER β . To test this possibility, DNA sequences encoding deletion mutants of the C terminus of ER β were transfected into 293 cells and levels of expressed protein were determined by Western blot analysis. When the F domain was deleted [ER β (Δ F)], a dramatic reduction in ER β protein was observed in the absence of estrogen (Fig. 6B). This reduction in ER β was inhibited by MG132, indicating that the F domain suppresses the proteasome-dependent degradation of ER β . The degradation of ER β (Δ F) required the DRD, because ER β (Δ DRD; Δ F) was not degraded in the absence of estrogen. In contrast, the degradation of ER β (Δ 140; Δ F) was enhanced by fusion with the DRD [ER β (DRD; Δ 140; Δ F)] in both the presence and the absence of estrogen (Fig. 6B). These results suggest that the F domain suppresses the DRD-dependent degradation of ER β in the absence of estrogen.

In contrast to what was seen for ER β , the deletion of the F domain in ER α did not affect its degradation. To study this, we generated a chimeric ER β , ER β (α F), in which the F domain was substituted with an ER α F domain. However, there is

almost no homology between the ER α F and ER β F domains, and the F domain of ER α was able to protect ER β from proteolysis in the absence of estrogen (Fig. 6B).

Next, we determined the ubiquitination statuses of ER β and ER β (Δ F). That of ER β (Δ F) was similar to that of full-length ER β (Fig. 7A), indicating that the F domain does not regulate the ubiquitination step of ER β . Thus, the F domain may inhibit the accession of 26S proteasome to ER β structurally. Therefore, we evaluated the binding between ER β and proteasomes. FLAG-tagged ER β or ER β (Δ F) was transfected into 293 cells with SUG-1, which is one of the components of regulatory subunit of 26S proteasome. A coimmunoprecipitation experiment revealed that deletion of the F domain enhanced association between ER β and SUG-1 (Fig. 7B). In addition, SUG-1 efficiently reduced ER β (Δ F) rather than ER β (Fig. 7C). Thus, in the absence of estrogen, the F domain appears to abrogate the binding of the 26S proteasome to ER β to protect the receptor from proteolysis.

Receptor degradation is involved in the downregulation of transcription of the gene for ER β after ligand withdrawal. Recent evidence indicates that receptor degradation is coupled to transactivation and that the transcriptional activity of the gene for ER α is abrogated by the addition of MG132. The transcriptional activity of ER β was also reduced by MG132 (Fig. 8A). Thus, it is likely that receptor degradation is necessary for the ligand-dependent transactivation of the ER β gene. To investigate the association between CHIP-mediated recep-

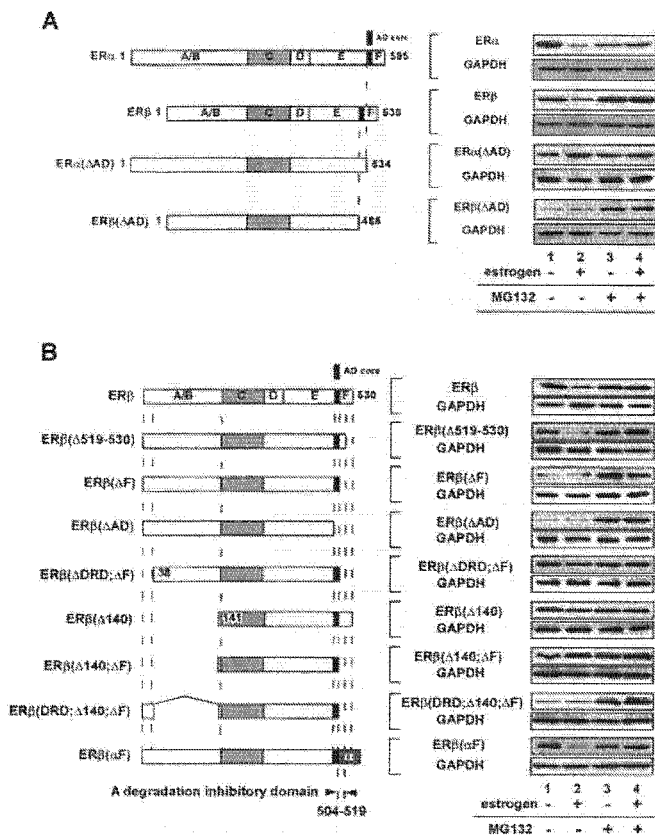


FIG. 6. The F domain suppresses DRD-mediated proteolysis of ER β . (A) AD core deletion in ER β increased the degradation of ligand-unbound receptor. DNA sequences (500 ng) encoding the indicated FLAG-tagged ER deletion mutants were transfected into 293 cells. These cells were cultured in the presence or the absence of estrogen (10^{-8} M) and MG132 (10^{-6} M). To evaluate the protein levels of the ER mutants, Western blot analysis was performed using anti-FLAG-M2 antibody. (B) F domain protects ER β from DRD-mediated degradation. DNA sequences (500 ng) encoding the indicated FLAG-tagged ER β deletion mutants were transfected into 293 cells cultured in the presence or the absence of estrogen (10^{-8} M) and MG132 (10^{-6} M). To evaluate the protein levels of the ER β mutants, Western blot analysis was performed using anti-FLAG-M2 antibody.

tor degradation and transactivation, we evaluated the transcriptional activities of ER β deletion mutants by use of a transient reporter assay. As shown in Fig. 8B, ER β (Δ DRD) exhibited a transcriptional activity higher than that of full-length ER β . However, ER β (Δ 140) still showed transcriptional activity. When the DRD was fused to ER β (Δ 140) to form ER β (DRD; Δ 140), its transcriptional activity was reduced (Fig. 8B). Similarly, ER β (Δ 140; Δ F) exhibited higher transcriptional activity than ER β (Δ F), but fusion of DRD decreased its transcriptional activity (Fig. 8B). In agreement with these results, CHIP expression downregulated the transcriptional activity of the ER β gene (Fig. 8C). In contrast, CHIP siRNA enhanced transcriptional activity (Fig. 8C). The transcriptional activity of ER β (Δ DRD) was not affected by expression of CHIP (Fig. 8C). Overall, our results indicate that CHIP-mediated degradation is not necessary for receptor-mediated transactivation. In addition, CHIP is able to ubiquitinate and to degrade ER β (mC) (Fig. 5A), indicating that binding to the DNA ele-

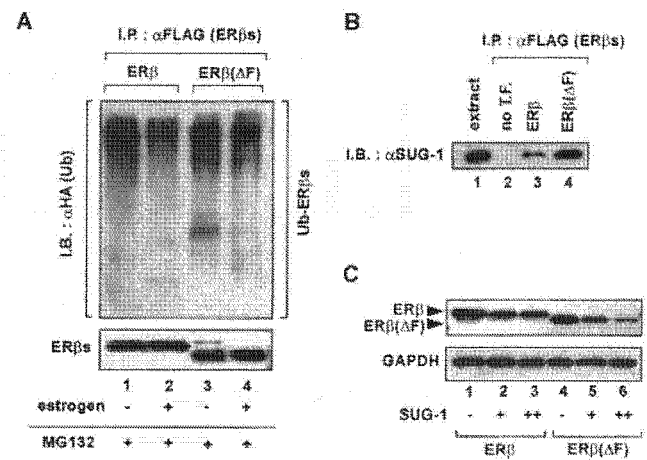


FIG. 7. F domain abrogates the association of proteasomes with ER β . (A) Deletion of the F domain does not alter the ubiquitination status of ER β . DNA sequences (500 ng) encoding the indicated FLAG-tagged ER β mutants and DNA (1,000 ng) encoding HA-tagged ubiquitin were transfected into 293 cells in the presence or the absence of estrogen (10^{-8} M). Upper panel: FLAG-tagged ER β mutants were immunoprecipitated (I.P.) with anti-FLAG-M2 antibody. The ubiquitination status of ER β was analyzed by use of Western blots probed with anti-HA antibody. I.B., Western blotting. Lower panel: immunoprecipitated ER β mutants were detected by use of Western blots probed with anti-FLAG antibody. (B) The F domain abrogates the association of SUG-1 with ER β . DNA sequences (500 ng) encoding either ER β or ER β (Δ F) were transfected into 293 cells. FLAG-tagged ER β or ER β mutants were immunoprecipitated with anti-FLAG-M2 antibody. The precipitates were Western blotted and probed with an antibody against SUG-1. T.F., transfection. (C) The F domain protects ER β from SUG-1-dependent degradation. DNA sequences (100 ng) encoding SUG-1 were cotransfected into 293 cells with or without DNA sequences (500 ng) encoding FLAG-tagged ER β or ER β (Δ F). The levels of ER β or ER β (Δ F) protein were examined by Western blotting and probed with anti-FLAG antibody.

ment is not necessary for CHIP-mediated receptor degradation. These results show that large amounts of liganded ER β protein are selectively and rapidly degraded independently of receptor-mediated transcription by CHIP.

To investigate the biological significance of this "wastefulness," we hypothesized that CHIP-mediated degradation selectively and rapidly degrades the active form of ER β to shut off ER β -mediated transcription when the estrogen dose is reduced. To test this hypothesis, we measured the transcriptional activities of constructs encoding ER β and ER β (Δ DRD) after estrogen withdrawal. DNA sequences encoding either ER β or ER β (Δ DRD) were transfected into 293 cells together with a plasmid in which the PEST sequence was fused to the luciferase gene (ERE-TATA-LucCP), and the luciferase activity was measured at various time points after estrogen withdrawal. As shown in Fig. 9A, the transcriptional activity of the ER β sequence was reduced much faster than that of ER β (Δ DRD). Using MDA-MB-231 cells that stably express either control siRNA or CHIP siRNA, we tested whether CHIP is involved in the downregulation of ER β -mediated transcription after reduction of the ligand dose. Plasmids containing the PEST-fused luciferase gene were transfected into MDA-MB-231 cells expressing either control siRNA or CHIP siRNA. ER β gene-mediated transcription was downregulated faster in the MDA-